

1  
2  
3  
4  
5  
6  
7  
8  
9  
10  
11  
12  
13  
14  
15  
16  
17  
18  
19  
20

**Sulphate partitioning into calcite: Experimental verification of pH control and application to seasonality in speleothems**

Peter M. Wynn<sup>a\*</sup>, Ian. J. Fairchild<sup>b</sup>, Andrea Borsato<sup>c</sup>, Christoph Spötl<sup>d</sup>, Adam Hartland<sup>e</sup>, Andy Baker<sup>f</sup>, Silvia Frisia<sup>c</sup>, James Baldini<sup>g</sup>

<sup>a</sup>*Lancaster Environment Centre, University of Lancaster, Lancaster, LA1 4YQ, UK.*

<sup>b</sup>*School of Geography, Earth and Environmental Sciences, University of Birmingham, Birmingham, Edgbaston, B15 2TT, UK*

<sup>c</sup>*School of Environmental and Life Sciences, The University of Newcastle, Callaghan, NSW 2308, Australia*

<sup>d</sup>*Institut für Geologie, Leopold-Franzens-Universität Innsbruck, Innrain 52, 6020 Innsbruck, Austria*

<sup>e</sup>*Environmental Research Institute, Science and Engineering, University of Waikato, Hamilton 3240, New Zealand*

<sup>f</sup>*Connected Waters Initiative Research Centre, UNSW Sydney, Sydney, NSW 2052, Australia.*

<sup>g</sup>*Department of Earth Sciences, University of Durham, Durham DH1 3LE, UK*

\* Corresponding author. Tel. +44(0)1524 510235. E-mail address: [p.wynn@lancaster.ac.uk](mailto:p.wynn@lancaster.ac.uk)

21 **Abstract**

22 Carbonate-associated sulphate (CAS) is a useful carrier of palaeoenvironmental information  
23 throughout the geologic record, particularly through its stable isotope composition. However, a  
24 paucity of experimental data restricts quantitative understanding of sulphate incorporation into  
25 carbonates, and consequently CAS concentrations and their diagenetic modifications are rarely  
26 interpreted. However, in the case of calcite speleothems, the remarkably high-resolution CAS  
27 records which are obtainable via modern microanalytical techniques represent a potentially  
28 invaluable source of palaeoenvironmental information. Here, we describe the results of controlled  
29 experiments of sulphate co-precipitation with calcite in freshwater solutions where pH, saturation  
30 state, and sulphate concentration were varied independently of each other. Solution pH is confirmed  
31 as the principal control on sulphate incorporation into calcite. The relative efficiency of  
32 incorporation was calculated as a partition coefficient  $D_{SO_4} = (m_{SO_4}/m_{CO_3})_{solid} / (m_{SO_4}/m_{CO_3})_{solution}$ .  
33 High crystal growth rates (driven by either pH or saturation state) encouraged higher values of  $D_{SO_4}$   
34 because of an increasing concentration of defect sites on crystal surfaces. At low growth rates,  $D_{SO_4}$   
35 was reduced due to an inferred competition between sulphate and bicarbonate at the calcite  
36 surface. These experimental results are applied to understand the incorporation of sulphate into  
37 speleothem calcite. The experimentally determined pH-dependence suggests that strong seasonal  
38 variations in cave air  $PCO_2$  could account for annual cycles in sulphate concentration observed in  
39 stalagmites. Our new experimentally determined values of  $D_{SO_4}$  were compared with  $D_{SO_4}$  values  
40 calculated from speleothem-drip water monitoring from two caves within the Austrian and Italian  
41 Alps. At Obir cave, Austria,  $D_{SO_4}$  ( $\times 10^5$ ) varies between 11.1 (winter) and 9.0 (summer) and the  
42 corresponding figures for Ernesto cave, Italy, are 15.4 (winter) and 14.9 (summer). These values  
43 approximate predicted  $D_{SO_4}$  values based on our chamber experiments containing both low (2 ppm)  
44 and high (20 ppm) sulphate concentrations. Our experimental values of  $D_{SO_4}$  obtained at crystal  
45 growth rates typical of stalagmites, closely match those observed in other cave sites from around  
46 the world. This validates the universality of the controls behind  $D_{SO_4}$  and will enhance the use of  
47 speleothem CAS as a palaeoenvironmental proxy.

48

49

50

## 51 Introduction

52 Carbonate-associated sulphate (CAS) has long been recognized as a tool for understanding past  
53 environmental processes (Burdett et al., 1989). Most literature focuses on its isotope composition in  
54 marine archives as being indicative of global processes affecting sulphur cycling (e.g. Bottrell and  
55 Newton, 2006; Rennie and Turchyn, 2014). Sulphur and oxygen isotope systematics of CAS have also  
56 been used in marine and freshwater environments to inform on regimes of high atmospheric PCO<sub>2</sub> in  
57 ancient time (Bao et al., 2008, 2009; Benn et al., 2015) and for more recent environments, sulphur  
58 isotope systematics of CAS in speleothems has been used to reconstruct loading of SO<sub>2</sub> emissions to  
59 the atmosphere (Wynn et al., 2008, 2010). However, in contrast to isotopic studies, interpretations  
60 based purely on CAS concentrations are more limited due to uncertainty surrounding the nature of  
61 sulphate incorporation into the carbonate lattice. Even though lattice-substitution of analogue ion  
62  $\text{SeO}_4^{2-}$  has been demonstrated by Reeder et al. (1994) and substitution of carbonate by sulphate was  
63 directly demonstrated by the X-ray absorption studies of Pingitore et al. (1995), the lack of a  
64 quantitative understanding of sulphate incorporation into carbonates currently limits interpretation.

65 The only experimental study on CAS incorporation was carried out by Busenburg & Plummer (1985)  
66 for marine-analogue systems. They interpreted results using a thermodynamic model in which a  
67 Berthelot-Nernst distribution coefficient (McIntyre, 1963) was defined as:

$$68 \quad 69 \quad D_{\text{SO}_4} = (\text{SO}_4/\text{CO}_3)_{\text{calcite}} / (\text{SO}_4/\text{CO}_3)_{\text{solution}} \quad (1)$$

70 This implied that sulphate incorporation was facilitated at lower pH where the ratio of aqueous CO<sub>3</sub><sup>2-</sup>  
71 /HCO<sub>3</sub><sup>-</sup> is lower. However, at the high ionic strength, fast growth rates and high absolute SO<sub>4</sub>  
72 concentrations of these experiments (100-10,000 ppm SO<sub>4</sub> in growth media), kinetic factors also  
73 influenced the system, and there was a strong correlation between the value of D<sub>SO<sub>4</sub></sub> and  
74 precipitation rate. When applied to a typical speleothem-forming site (Frisia et al., 2005), these  
75 experimental results under-predicted S abundance in speleothem calcite by an order of magnitude.  
76 This mismatch was the impetus for the current study to derive experimental data representative of  
77 freshwater environments.

78 The sulphate content of speleothem carbonate has recently become appreciated as a valuable  
79 record of the changing sulphur biogeochemical cycle at a local to regional scale. Where atmospheric  
80 sulphur is deposited through precipitation, and cycling of sulphur through the biomass above the  
81 cave can be accounted for, secular trends in speleothem sulphur content can record regional  
82 pollution characteristics (Frisia et al., 2005; Wynn et al., 2008, 2010; Uchida et al., 2013), as well as  
83 infer volcanic events (Frisia et al., 2008; Badertscher et al., 2014) and periods of biomass burning  
84 (Nagra et al., 2016; Treble et al., 2016). However, beyond the long-term trends in speleothem  
85 sulphur content, there is much information still to be revealed by addressing sulphur dynamics at  
86 the sub-annual scale. When analysing speleothem sulphate content at high resolution, a clear high-  
87 resolution cyclicity is revealed despite minimal short-term variation in the sulphate content of the  
88 associated drip waters (Frisia et al., 2005; Fairchild et al., 2010; Wynn et al., 2014). The driver behind  
89 such high-resolution speleothem sulphate dynamics must therefore be associated with processes of  
90 sulphate incorporation during carbonate precipitation and speleothem growth.

91 It is well established that seasonal variation in  $\text{PCO}_2$  of cave air has a direct effect on the rate of  
92 speleothem carbonate deposition. In most temperate caves, strong density-driven winter air  
93 circulation lowers cave air  $\text{PCO}_2$  (Fairchild and Baker, 2012; James et al., 2015). These conditions will  
94 promote drip water degassing, consequently increasing drip water pH and calcite saturation state.  
95 Cave air  $\text{PCO}_2$  therefore drives variability in drip water carbonate content and (in the absence of  
96 strong changes in drip rate) speleothem growth rate within an annual cycle. Following the  
97 arguments of Busenberg and Plummer (1985), a pH-driven variation in CAS incorporation should  
98 occur such that sulphate incorporation is dependent upon the ratio to carbonate ions in solution. If  
99 cave air  $\text{PCO}_2$  varies seasonally, this should give rise to cyclicity in speleothem sulphate content with  
100 low winter and high summer concentrations which are independent of cave drip water sulphate  
101 content. Independent markers of seasonality in some caves are provided by annual flushes of  
102 fluorescent organic matter with associated colloids (Baker et al., 2008; Fairchild and Baker, 2012).  
103 Using such markers, seasonal  $\text{SO}_4$  cycles (a winter trough and a summer peak) in speleothems from  
104 two Alpine caves have been found to be in qualitative agreement with changes in cave air  $\text{PCO}_2$   
105 (Fairchild et al., 2010; Wynn et al., 2014) (Figure 1).

106 To test this theory of sulphate incorporation into speleothem calcite, we use our experimental set-  
107 up to simulate the partitioning of sulphate between aqueous media and carbonate deposits under  
108 conditions appropriate to dilute cave waters, such as has been carried out on other species (Huang  
109 and Fairchild, 2001; Day and Henderson, 2013). A novel feature of the experimental design is the  
110 ability to control calcite supersaturation and pH independently, in order to distinguish these as  
111 controlling variables. We also use two different sulphate concentrations covering the range typically  
112 found in cave drip waters. Experimental results are compared to two European Alpine caves: Obir  
113 Cave (Spötl et al., 2005; Fairchild et al., 2010), Austria; and Grotta di Ernesto (Frisia et al., 2005;  
114 Borsato et al., 2007; Wynn et al., 2010, 2013), Italy, where sample analysis at high temporal  
115 resolution demonstrates the seasonality of sulphate partitioning between cave waters and  
116 speleothem calcite. Summary data from other globally-distributed cave sites also allow calculation of  
117 partition co-efficients between sulphur contained in drip waters and speleothem calcite, albeit at a  
118 lower temporal resolution. In all cave sites, values of in-cave  $D_{\text{SO}_4}$  are close to the experimental data,  
119 which suggests a universal set of controls on the efficiency of sulphate incorporation into  
120 speleothem calcite, governed primarily by pH, aqueous sulphate concentration and growth rate.

121

## 122 **Methodology**

### 123 ***Carbonate crystal growth experiments***

124 A simple experimental design was adopted in which solutions of defined calcite supersaturation  
125 were seeded with calcite crystals. Solutions were left to precipitate, with the aim of producing a  
126 fairly constant rate of growth for each experiment, within the range of growth equating to typical  
127 rates of linear extension for stalagmites (20-1000  $\mu\text{m}/\text{year}$ ) (McDermott et al., 1999).

128 Experiments were designed to cover a range of calcite saturation states and pH (Fig. 2 and Fig S1).  
129 Multiple experiments were carried out simultaneously in gas-tight Pyrex© bottles of either 1 L or 0.5  
130 L volume with a headspace of 120 ml. The existence of a headspace helps maintain supersaturation  
131 by permitting degassing of carbon dioxide. Following Henry's Law, the maximum moles of  $\text{CO}_2$

132 degassed are calculated to be only 3% of total moles of CaCO<sub>3</sub> precipitated as most of the CO<sub>2</sub>  
133 generated remains in solution. Growth media were prepared from a mixed stock solution to produce  
134 different solution concentrations containing CaCl<sub>2</sub> and NaHCO<sub>3</sub> as follows: C1N1 = CaCl<sub>2</sub> (3.5mM) and  
135 NaHCO<sub>3</sub> (7mM); C05N05 = CaCl<sub>2</sub> (1.75mM) and NaHCO<sub>3</sub> (3.5mM); and C1.5N1.5 = CaCl<sub>2</sub> (5.25mM)  
136 and NaHCO<sub>3</sub> (10.5mM). The pH of each starting solution was then adjusted by addition of HCl or  
137 NaOH to achieve the compositions shown in Fig. 2 (equivalent PCO<sub>2</sub> values are shown in Fig. S1).  
138 Seed crystals of calcite were grown from a solution of 0.8 M NaHCO<sub>3</sub> and 0.4 M CaCl<sub>2</sub> resulting in  
139 rhombic crystals ca. 18 μm diameter, with specific surface area of 0.15m<sup>2</sup>/g. Each experiment was  
140 doped with sulphate (as sodium sulphate solution) to produce a final growth media concentration of  
141 either 2 mg/L (0.02 mM) (low-sulphate experiments) or 20 mg/L (0.2 mM) (high-sulphate  
142 experiments). See Table 1 for the full range of experimental conditions.

143 After preparation of growth media, addition of seed crystals and adjustment of pH to the desired  
144 starting value, chambers were left to precipitate CaCO<sub>3</sub>. During the process of calcium carbonate  
145 precipitation, electrical conductivity (EC) declined due to the removal of calcium and carbonate ions  
146 from solution, and pH was lowered by the production of CO<sub>2</sub>. EC was measured using a Tetracon 325  
147 conductivity probe and WTW 340i combination meter, ref 25°C. pH was monitored using a Hamilton  
148 Liq-glass™ electrode and WTW 340i meter automatically compensated to a reference temperature  
149 of 25°C and calibrated to buffer solutions of pH 4.0 and 7.01 on use (precision +/- 0.01 pH units  
150 within two units from the calibration point). pH values were measured without stirring, and  
151 considered stable following no change to the measurement after approximately 30 seconds (WTW  
152 auto-read function) (cf. Leito et al., 2002). The chemical changes were modelled using geochemical  
153 speciation software MIX4 (Plummer et al., 1975; Fairchild and Baker, 2012) and compared to  
154 changes in electroconductivity calculated using algorithms of Rossum et al. (1975) and Hughes et al.  
155 (1994). The change in Ca<sup>2+</sup>(aq) and CO<sub>3</sub><sup>2-</sup>(aq) composition in each growth chamber was calculated  
156 based on this established relationship between ionic strength with both pH and EC. Results showed  
157 some scatter around the calculated co-variation in these parameters (Fig. S2) and pH results were  
158 preferred because of the better analytical precision in relation to the magnitude of change. To  
159 compensate for these changes in solution composition and re-adjust the saturation state back to the  
160 original starting value, addition of 0.1 M NaOH was used to adjust the pH, and a mixed restoration  
161 solution of 0.1 M CaCl<sub>2</sub> and 0.2 M NaHCO<sub>3</sub> was used to replenish the Ca<sup>2+</sup>, HCO<sub>3</sub><sup>-</sup> and CO<sub>3</sub><sup>2-</sup> ions in  
162 solution. Intervention with NaOH and restoration solution was undertaken on a daily or weekly  
163 timescale, dependent upon saturation state of the growth media and the rapidity of calcite  
164 precipitation. An example of an experiment with a weekly intervention is illustrated in Fig. 3: pH is  
165 repeatedly restored to the original value, but EC gradually rises because of accumulation of excess  
166 NaCl in solution. The change in pH prior to restoration was usually <0.1, but infrequently up to a  
167 maximum of 0.3, and the calcite saturation index ( $\Omega = \log$  ionic activity product over solubility  
168 product) was, correspondingly, lowered by 0.1-0.3.

169 Growth chambers were maintained until sufficient calcium carbonate had precipitated from solution  
170 for analysis. The precipitates were recovered from growth chambers by filtration. Crystals were  
171 imaged by Scanning Electron Microscopy (SEM), and rates of growth calculated by conversion of  
172 CaCO<sub>3</sub> precipitated (mg) during each experiment, to rates of linear extension in mm yr<sup>-1</sup>. Crystal  
173 growth rates were similar to a sub-set of those of Mucci and Morse (1983) where calcite was grown  
174 under similar saturation states and Mg/Ca ratios (Fig. S3). Each of the recovered aliquots of calcite  
175 crystals were digested in 8 ml of 2 % v/v HNO<sub>3</sub> (Aristar grade) and sulphur concentrations were

176 determined by high-resolution inductively coupled plasma mass spectrometric analysis (HR-ICPMS)  
177 at Kingston University, UK, using methods described in Frisia et al. (2005). Calibration solutions at 1,  
178 5, 10, 20, 50 and 100 ppb were diluted from a stock reference material of 1000 ppm sodium  
179 sulphate solution. Repeat analysis of the 10 ppb reference standard, tested as an unknown solution  
180 gave a sample precision to within <5% of the known concentration. Drift was monitored throughout  
181 the analytical sequence. Allowing for the mass of sulphate-free seed, the corrected sulphate  
182 concentration was determined and  $D_{SO_4}$  calculated from this value and the solution composition.

183

#### 184 ***Cave site and speleothem sample descriptions***

185 One speleothem was studied from each of two Alpine locations. Obir cave (SE Austria) lies within the  
186 Triassic limestone of the Obir Massif (46°30'36"N, 14°32'24"E, ~1100 m a.s.l.). The vegetation above  
187 the cave system is characterised by mixed deciduous / coniferous forest and well-developed brown  
188 earth soil extends to a depth of approximately 30 cm above the cave. Cave internal temperatures  
189 are +5.7 +/- 0.1°C and strong cave ventilation reflects the dominant seasonality of cave external  
190 temperatures (Spötl et al., 2005). Speleothem Obi84 was collected during 2002 and speleothem  
191 Obi12 was collected in 1998. Both samples have subsequently become noted for their seasonality of  
192 texture and geochemistry (Smith et al., 2009; Fairchild et al., 2010). Sulphur variations in speleothem  
193 Obi84 are apparent on both centennial and sub-annual scales (Wynn et al., 2010; Wynn et al., 2014).  
194 The Ernesto cave system lies 220 km to the WSW (45°58'37"N, 11°39'28"E, 1167 m a.s.l.) within the  
195 partially dolomitised Jurassic limestones of NE Italy. A similar vegetation composition of mixed  
196 deciduous / coniferous forest supports a clay-rich calcareous brown soil 0.5 - 1.5 m thick above the  
197 cave. The internal cave temperature is +6.7 +/-0.1 °C (Miorandi et al., 2010), and a strong  
198 seasonality in external temperature drives a cave ventilation pattern which holds a dominant  
199 influence over the cave carbon budget and speleothem growth patterns (Frisia et al., 2011).  
200 Speleothem ER78 was collected in 2000 and has been studied extensively for its sulphur content  
201 (Frisia et al., 2005; Wynn et al., 2010) and associated biogeochemical cycling of sulphur through the  
202 cave and overlying ecosystem (Wynn et al., 2013; Borsato et al., 2015).

203 Due to the broad similarities in climate regime, vegetation composition and cave ventilation  
204 dynamics at each cave site, both speleothems display similar trends in sulphur dynamics over the  
205 past 100 years. Analysis of both speleothem samples for sulphur content was undertaken at the  
206 European Synchrotron Radiation Facility (ESRF) at beamline ID21 in 2011 (Obi84) and 2003 (ER78).  
207 Analytical details are reported in Wynn et al. (2014) and Frisia et al. (2005) respectively. A rise in  
208 sulphur concentration throughout the 20<sup>th</sup> century is commensurate with a shift in isotopic  
209 composition signifying enhanced fossil fuel emissions (Wynn et al., 2010). Maximum concentrations  
210 of sulphur within each speleothem lag peak atmospheric emissions from industrialisation by  
211 approximately 10-15 years, attributed to biogeochemical attenuation within the overlying  
212 vegetation (Frisia et al., 2005; Wynn et al., 2010; Wynn et al., 2013). High-resolution variability in  
213 sulphur concentration in the form of annual cycles, is superimposed on the long-term centennial  
214 sulphur trend in each speleothem (Frisia et al., 2005; Wynn et al., 2014). Cycles in sulphur  
215 concentration were confirmed as annual, based on the use of an age model for each speleothem  
216 developed using U-Th dating, visible lamina counting, and automated peak detection software  
217 developed by Smith et al. (2009). Annual pulses in Zn associated with colloidal movement during

218 periods of April/September water excess for speleothem Obi84 (Fairchild et al., 2010; Hartland et al.,  
219 2011; Hartland et al., 2012), and broadly synchronous changes in P (for speleothem ER78) (cf. Frisia  
220 et al., 2005; Borsato et al., 2007; Smith et al., 2009) were also used to further delimit the annual  
221 nature of sulphur cycles. Other cave sites where coeval speleothem extraction and drip water  
222 chemical monitoring allow the calculation of site-specific  $D_{SO_4}$  values include: Rukiesa cave, Ethiopia;  
223 Crag Cave, Ireland; Uamh An Tartair, Scotland, UK; Browns Folly Mine, UK; Shimizu-do cave, Japan;  
224 and Ryuo-do cave, Japan. For each of these sites, drip water chemical monitoring is at a resolution  
225 lower than seasonal, and speleothem sulphur concentrations were determined only at low  
226 resolution incorporating several years of carbonate deposition from the most recent growth. Details  
227 of each of these sites is provided in the supplementary information.

228

## 229 **Results**

230 Results from the growth chamber experiments are presented in Table 1, demonstrating the controls  
231 on sulphate incorporation into calcite. The pH control on absolute concentrations of sulphate  
232 incorporated during crystal growth is demonstrated in Fig. 4a. A negative relationship between  
233 sulphur concentration in calcite overgrowths and the pH of the growth media is apparent at high (20  
234 ppm) concentrations of sulphate contained within the growth solution ( $p=0.044$ ). This is consistent  
235 with the assumption that competition between sulphate and carbonate ions would force low levels  
236 of sulphate incorporation at high pH. The pH dependence of sulphate incorporation into calcite is  
237 limited in growth media of low sulphur concentration.

238 The substitution of carbonate by sulphate within the calcium carbonate lattice (Equation 1) suggests  
239 that elevated carbonate ion concentrations discourage sulphate incorporation. Therefore, sulphate  
240 incorporation rates should decrease by an order of magnitude relative to unit increases in pH (pH  
241 being an exponential scale, an increase in pH by one unit increases the  $CO_3/HCO_3$  ratio by a factor of  
242 10). However, sulphate incorporation only changes by a factor of 3 for every pH unit at 20 ppm  
243 aqueous sulphate and less than a factor of 2 for every pH unit at 2 ppm aqueous sulphate. This  
244 therefore results in a  $D_{SO_4}$  which increases with pH, suggesting a more efficient incorporation of  
245 sulphate into calcite at high pH and at low sulphur concentration (Fig. 4b,  $p<0.02$  for high (20 ppm)  
246 and  $p=0.05$  for low (2 ppm) experimental series). A comparison of solutions with similar pH and  
247 differing saturation states reveals that the same positive relationship to D is expressed (Fig. 5,  
248  $p=0.05$ ). Conditions of high pH, high supersaturation (driven independently of pH), and low sulphur  
249 concentration within experimental solutions thereby appear to promote a greater efficiency of  
250 sulphate incorporation into carbonate crystals.

251 Where records from cave drip water/pool water and speleothem sulphate analyses overlap,  
252 partition coefficients (expressed as values of  $D_{SO_4}$ ) have been calculated. These are presented in  
253 Table 2 as average seasonal values for the Obir and Ernesto cave sites, and can be compared to the  
254 experimental data. Analysis of in-cave partition coefficients is also extended to cave sites in other  
255 regions where coeval aqueous and speleothem carbonate sulphate analysis has been undertaken,  
256 albeit at a lower resolution of analysis (Tables 3-4).

257

258 **Discussion**

259 **Mechanisms of sulphate incorporation into experimental calcite**

260 Sulphate incorporation into calcite has traditionally been determined to proceed by sulphate acting  
261 as a substituent for carbonate. Partition coefficients, expressed as  $D_{SO_4}$  (equation 1) have thereby  
262 depicted the incorporation of sulphate to be driven at least in part by the aqueous  $SO_4/CO_3$  ratio,  
263 controlled by pH and saturation state (Busenburg and Plummer, 1985). This relationship has been  
264 proved correct in a qualitative fashion (Fig 4a), demonstrating the sulphate content of experimental  
265 calcite to decline with increasing pH when aqueous sulphate concentrations approximate 20 ppm.  
266 However, when aqueous sulphate concentrations approximate 2 ppm, the pH and saturation state  
267 control on sulphate incorporation into calcite is weak. This limited relationship reflects two  
268 confounding factors which expose the weakness of  $D_{SO_4}$  as a universal parameter, and reflect the  
269 deficiencies of the partition coefficient approach (Fairchild and Baker, 2012, ch.8). These can be  
270 summarised as follows: 1.  $D_{SO_4}$  increases with pH (Fig. 4b), offsetting the expected decline in calcite  
271 sulphate content (Equation 1). 2. At constant pH, growth rate is driven by supersaturation and an  
272 associated increase in  $D_{SO_4}$ , with growth rate is demonstrated (Figs. 5a,b). These deviations from the  
273 partition co-efficient approach suggest multiple controls to anion substitution into calcium  
274 carbonate (cf. Uchikawa et al., 2017) indicating a dual model to sulphate incorporation comprising A.  
275 Substitution of carbonate for sulphate following partition coefficient behaviour (cf. Busenburg and  
276 Plummer, 1985), albeit modified to account for the effects of bicarbonate competition on the calcite  
277 surface (Andersson et al., 2016); and B. Possible incorporation of sulphate into the solid-state lattice  
278 at defect sites (cf. Pingitore and Eastman, 1986; Staudt et al., 1994).

279 *Bicarbonate competition on the calcite surface:* Traditional models of partition co-efficient behaviour  
280 concerning carbonate ion abundance do not consider the effects of a bicarbonate competition for  
281 space within the calcite lattice. The partition co-efficient ( $D_{SO_4}$ ), as defined through Equation 1,  
282 assumes all carbonate which contributes to the growth of calcite crystals is deposited directly onto  
283 the growth surface as  $CO_3^{2-}$  ions (Equation 1). However, both  $HCO_3^-$  and  $CO_3^{2-}$  are capable of  
284 contributing to calcite growth, by diffusing towards and attaching to the growth surface of  $CaCO_3$   
285 crystals (eg. Przybylinski, 1987; Van der Weijden et al., 1997; Van der Weijden et al., 2014). The  
286 subsequent deprotonation of bicarbonate adsorbed to and/or incorporated within the calcite lattice  
287 to produce carbonate ions has a  $pK_a$  value which is less than free bicarbonate in solution (Andersson  
288 et al., 2016). This means the calcite surface preferentially stabilizes carbonate ions relative to  
289 bicarbonate, leaving only low concentrations of bicarbonate ions present within the lattice (Feng et  
290 al., 2006) despite much higher concentrations within the aqueous phase. The values of  $pK_a$  for  
291 deprotonation of  $HCO_3^-$  to  $CO_3^{2-}$  on the surface of calcite vary by six orders of magnitude depending on  
292 pH and calcite surface geometry. However, at the pH values present within natural cave  
293 environments (encompassing those used within the present study), values of  $pK_a$  suggest virtually  
294 complete deprotonation regardless of calcite surface conditions (Andersson et al., 2016). This leads  
295 to competition between bicarbonate and sulphate for space within the calcite lattice, which is  
296 determined by solution pH and relative bicarbonate ion abundance. At high pH (higher than 10.3),  
297 where carbonate ions in solution are more abundant, the effects of bicarbonate competition are  
298 limited and  $D_{SO_4}$  should be close to the true value as calculated through equation 1. At the range of  
299 pH conditions conducive to a greater dominance of bicarbonate ions in solution (between pH 6.4  
300 and 10.3), 'bicarbonate competition' with sulphate for spaces within the calcite lattice serves to

301 dilute the incorporation of the sulphate molecule, thereby introducing uncertainty into the partition  
302 coefficient calculation of Equation 1. This results in a lower  $D_{SO_4}$  than expected from Equation 1 and  
303 reflects the relationship to pH depicted through Figure 4b.

304 *Defect site abundance:* The abundance of defect sites in calcium carbonate crystals is directly related  
305 to supersaturation state and therefore crystal nucleation and growth (McDermott et al., 1999; Frisia  
306 et al., 2000). An enhanced presence of defect sites (visible as stepped crystal faces) is known to  
307 encourage exchange of ions between aqueous and solid phases (Pingitore and Eastman, 1986;  
308 Staudt et al., 1994; Borsato et al., 2016; Uchikawa et al., 2017). Therefore, increased defect site  
309 density at higher supersaturation states promotes sulphate incorporation (increasing  $D_{SO_4}$ ) (Figure  
310 6), and is manifested through increasing  $D_{SO_4}$  with both pH (Fig 4b) and higher growth rates when pH  
311 remains constant (Figs. 5a-b).

312 The net effects of all these processes (partitioning according to carbonate ion abundance;  
313 competition with bicarbonate; the presence of defect sites; and the absolute concentrations of  
314 sulphate in solution) are depicted through Fig. 7. The apparent increase in calcite sulphur content  
315 with growth rate (Fig. 7) is counter-intuitive based on a model of sulphate incorporation controlled  
316 solely by carbonate ion abundance in solution (Equation 1). Instead, sulphate incorporation at defect  
317 sites must increase  $D_{SO_4}$  and offset the effects of carbonate ion abundance. The strength of this  
318 overall growth rate effect is modest, exhibiting a ~20% increase in sulphur concentration in calcite  
319 over an order of magnitude growth rate increase along a line of constant pH (at 20 ppm sulphate  
320 solution,  $p=0.05$ ). At lower sulphate concentrations in solution (2 ppm), the same effect of enhanced  
321 sulphur incorporation into calcite with growth rate offsets the expected dilution by carbonate ion  
322 abundance but does not display a positive trend. At similar rates of growth, the effect of pH upon  
323 sulphur incorporation into calcite follows the relationship depicted through figure 4a, whereby pH  
324 control of aqueous  $SO_4/CO_3$  ratio determines the abundance of sulphate incorporated into calcite  
325 despite any effects of variable  $D_{SO_4}$ .

326

### 327 **Comparison to published experimental data**

328 The only other study to date investigating partitioning of sulphate into calcite (Busenberg and  
329 Plummer, 1985) addressed crystal growth rates predominantly faster than those encountered during  
330 speleothem deposition (linear extension rates equivalent to 0.3 to 40 mm/year). Additionally,  
331 experimental solutions used concentrations of sulphate and sodium one to two orders of magnitude  
332 greater than those typical of karst environments. The relationship between crystal growth rate and  
333 partition coefficient is depicted through Fig. 8 as a linear expression relating LOG(D) to LOG(R)  
334 ( $p=9.0 \times 10^{-13}$ , where LOG(R) is LOG growth rate in mm extension per year).

$$335 \text{ LOG(D)} = 0.8098 * \text{LOG(R)} - 0.1446 \quad (2)$$

336 Extrapolating the linear relationship in Equation 2 to a growth rate of  $100 \mu\text{m yr}^{-1}$ , should yield a  $D_{SO_4}$   
337 value ( $\times 10^5$ ) of 0.1. This is much lower than the values of  $D_{SO_4}$  obtained as a part of this study for  
338 similar rates of growth. At low (2 ppm) sulphur concentrations,  $D_{SO_4} \times 10^5 = 32.9$ , whereas at higher  
339 concentrations of sulphate (20 ppm),  $D_{SO_4} \times 10^5 = 10.3$ . The greater efficiency of trace element  
340 incorporation in this study and at lower concentrations of sulphate may reflect the lower ionic

341 strength of the growth media. Difficulties in extrapolating partition coefficients beyond the studied  
342 range of solution composition has also been demonstrated for other trace elements such as Sr, Cd,  
343 Mn and Co during incorporation into calcite (e.g. Lorens, 1981).

344

#### 345 **Mechanisms of sulphate incorporation into speleothem calcite**

346 The proposed model of pH and defect control on sulphate incorporation into experimental calcite is  
347 consistent with observations of sulphate variability contained within speleothem carbonate. Where  
348 cave ventilation serves as the main driver of drip water pH, the incorporation of sulphate into the  
349 speleothem is modulated according to levels of CO<sub>2</sub> in the cave atmosphere (Frisia et al., 2005).  
350 Where ventilation occurs on a seasonal basis, this process gives rise to annual cycles of speleothem  
351 sulphate content despite relatively constant sulphate concentrations within cave drip waters across  
352 an annual cycle (Borsato et al., 2015). Minimal amounts of sulphate incorporation into speleothem  
353 carbonate always occur during ingress of external air with low PCO<sub>2</sub> into the cave chamber  
354 (therefore drip waters de-gas to attain a relatively high pH), and maximum levels of sulphate are  
355 incorporated in speleothem carbonate during egress of cave air when high ambient levels of cave air  
356 CO<sub>2</sub> reduce drip water degassing and thus limit the pH attained to lower values. At the Obir and  
357 Ernesto cave systems, this gives rise to a winter low and a summer high in speleothem sulphate  
358 concentration. However, if pH-determined sulphate substitution for carbonate were the sole  
359 controlling variable on sulphate incorporation into calcite, the seasonal cycle of speleothem sulphate  
360 would be expected to demonstrate a rapid switch between max and min concentrations in  
361 accordance with the rapidity of changes in cave ventilation regime. In reality, when analysed at high  
362 resolution (1 µm spatial resolution), the annual sulphate cycle appears blurred between max and  
363 min concentrations, contrasting with very sharp colloidal element bands (Fig. 1). This is likely due to  
364 gradual changes in the crystal growth surface and defect site availability, transitioning from high  
365 abundance of defects during the winter season to fewer defects during the summer over a time  
366 period which is slower than the switch in cave air CO<sub>2</sub> concentration (*sensu* Pingitore and Eastman,  
367 1986; Borsato et al., 2016). This is associated with classic seasonal changes in the morphology of  
368 crystals growing on glass plates beneath drips in Ernesto cave (Frisia et al., 2000). Seasonally  
369 modulated supersaturation control on defect site availability and therefore  $D_{SO_4}$ , thereby serves to  
370 modify the dominant pH control on sulphate substitution for carbonate.

#### 371 **In-cave partitioning of sulphate between cave water and speleothem calcite**

372 Where time series of cave pool water / drip water chemical analyses are temporally closely matched  
373 to speleothem records of sulphur concentration, the calculated partition coefficients between cave  
374 waters and speleothem calcite are directly comparable with those calculated through growth  
375 chamber experiments. This is undertaken at the Obir and Ernesto caves, where the frequency of drip  
376 water collection and the high resolution of speleothem sulphur analysis allow determination of  $D_{SO_4}$   
377 on a seasonal basis.

378 The seasonality of dripwater SO<sub>4</sub>/CO<sub>3</sub> characteristics reflect the cave ventilation dynamics (and  
379 thereby dripwater pH) at each site. At Obir cave, drip waters feeding speleothem Obi84 demonstrate  
380 a strong seasonality in drip water pH and SO<sub>4</sub>/CO<sub>3</sub> ratios. During the winter season (defined as  
381 October – March), higher pH and consequently lower SO<sub>4</sub>/CO<sub>3</sub> (mean pH = 8.3, mean SO<sub>4</sub>/CO<sub>3</sub> = 1.2)

382 contrasts with those values from the summer season (mean pH = 8.15, mean  $\text{SO}_4/\text{CO}_3 = 1.6$ ) (Table  
383 2). In Ernesto cave, calculations were performed on waters collected from Pool S1, the closest  
384 sampling site in the cave to the drip which fed stalagmite ER78. Seasonality in pH and  $\text{SO}_4/\text{CO}_3$  ratios  
385 reflect a similar pattern of cave ventilation-modulated carbonate precipitation as that found in Obir  
386 cave. During the winter season, pool water chemistry dictates a lower  $\text{SO}_4/\text{CO}_3$  ratio as a result of  
387 elevated pH and  $\Omega$  (mean pH = 8.14, mean  $\text{SO}_4/\text{CO}_3 = 2.7$ ). During the summer, lower drip water pH  
388 and  $\Omega$  result in a higher  $\text{SO}_4/\text{CO}_3$  ratio (mean pH = 8.0, mean  $\text{SO}_4/\text{CO}_3 = 3.8$ ) (Table 2). This variability  
389 in pH and  $\text{SO}_4/\text{CO}_3$  ratio drives the seasonally modulated cycles of speleothem sulphate as discussed  
390 above.

391 To enable sulphate partition co-efficients to be calculated between dripwaters and speleothem  
392 calcite, values of sulphate concentration in speleothem calcite were obtained at high resolution  
393 using raw counts generated by synchrotron XRF calibrated to analyses undertaken by secondary  
394 ionisation mass spectrometry (for speleothem Obi84) (Wynn et al., 2010) and high resolution ICPMS  
395 (for speleothem ER78) (Frisia et al., 2005). Concentrations of sulphate incorporated into speleothem  
396 calcite during the summer and winter seasons of each respective year were calculated as mean  
397 values based on the understanding that drip water Ca concentration indicates a 1.8x slower  
398 speleothem growth rate during the summer season. For Obi84, drip water chemistry from 2002-  
399 2004 is compared to speleothem sulphate concentrations from the nearest full annual cycle in the  
400 synchrotron sulphur profile (year 2000). For ER78, drip water chemistry monitored between 1996-  
401 1997 is compared only to the year 1996 due to a poor cyclical structure in the synchrotron sulphur  
402 profile from 1997. Based on the growth chamber experiments reported above, partitioning of  
403 sulphate between cave waters and speleothem calcite should follow a relationship such that values  
404 of  $D_{\text{SO}_4}$  are enhanced at higher pH. At Obir cave, values of  $D_{\text{SO}_4}$  ( $\times 10^5$ ) range between a winter mean  
405 of 11.1 to summer mean of 9.0 (Table 2,  $p=0.045$ ). At Ernesto cave, seasonal mean values of  $D_{\text{SO}_4}$   
406 ( $\times 10^5$ ) are calculated as 15.4 (winter) and 14.9 (summer), albeit statistically indistinguishable  
407 between summer and winter seasons. These values are close to the predicted values of  $D_{\text{SO}_4}$  based  
408 on chamber experiments containing both low (2 ppm) and high (20 ppm) sulphate concentrations  
409 and with crystal growth rates extrapolated to equivalent rates of linear extension (Table 2).

410 The partition co-efficients calculated between drip water and speleothem calcite can be interpreted  
411 based on experimental observations. Despite the lower concentrations of sulphate incorporated into  
412 speleothem calcite at higher pH values during the winter season (hence the origin of the annual  
413 speleothem sulphur cycles), values of  $D_{\text{SO}_4}$  reflect a greater efficiency of sulphate incorporation. This  
414 is hypothesized above to be due to an enhanced proportion of defects and kink sites at high levels of  
415 supersaturation that accommodate the sulphate ion (cf. Staudt et al., 1994). The increasingly  
416 defect-rich nature of crystal faces with increasing supersaturation state closely resembles processes  
417 of in-cave crystal formation, whereby winter growth at higher supersaturation promotes the  
418 formation of crystals with macro-kinks and steps (Frisia et al., 2000). However, given the modest  
419 increase in the sulphate content of experimental calcites over an order of magnitude increase in  
420 growth rate at constant pH (Fig. 7), the enhanced incorporation of sulphate at defect sites will not  
421 significantly diminish the over-riding pH control on  $\text{SO}_4/\text{CO}_3^-$  in product calcite. The growth chamber  
422 experiments of this study and Busenberg and Plummer (1985), thereby support a seasonality to  
423 sulphate incorporation in the speleothem record by identifying drip water pH (and by implication a  
424 pH-driven speleothem growth rate) as the key variable in determining the seasonality to sulphate  
425 incorporation and the magnitude of the partition coefficient ( $D_{\text{SO}_4}$ ).

426 **Universal applicability of speleothem  $D_{SO_4}$**

427 The universal applicability of  $D_{SO_4}$  to speleothems growing within the experimental range of crystal  
428 growth rates and aqueous sulphate concentrations is demonstrated in Table 3. For each speleothem,  
429  $D_{SO_4}$  is derived from field data collected at low temporal sampling resolution. Drip water chemical  
430 composition (pH, carbonate and sulphate content) is reported as annual mean values broadly  
431 contemporaneous with the date of speleothem collection. Speleothem growth rate is reported as an  
432 annual average value over the past 100 years, and sulphate content is reported from the most  
433 recent speleothem growth. Each calculated value of mean speleothem  $D_{SO_4}$  is seen to lie close to the  
434 range of experimentally determined partition coefficients when extrapolated to equivalent growth  
435 rates (Fig. 8) at low (2 ppm) and high (20 ppm) aqueous sulphate concentrations. The partitioning of  
436 sulphate between cave waters and speleothem calcite thereby appears to conform to  
437 experimentally determined controls across a range of environmental settings and temporal scales.

438 **Speleothem sulphate concentrations as indicators of past climatic variability**

439 The pH-dependence of sulphate incorporation into calcite and the universal relationship between  
440 growth rate (expressed as  $\text{mm yr}^{-1}$  linear extension) and  $D_{SO_4}$ , are two important findings which  
441 should permit the application of speleothem sulphate concentrations as climate proxies. These  
442 findings can be detailed as: 1. In a cave setting, the pH to which drip waters degas is controlled by  
443 the  $p\text{CO}_2$  of the cave air and therefore ventilation regime. The shape of each seasonal sulphate cycle  
444 (specifically cycle length) observed in speleothem calcite should therefore reflect the nature and  
445 timing of ventilation at each site. At sites where temperature-driven density differences control cave  
446 air  $p\text{CO}_2$ , a temperature decline occurring unusually early in the autumn or a temperature rise  
447 unusually late in the spring would produce an extended winter circulation pattern associated with  
448 low sulphate levels and an associated change in the morphology of the sulphur peak-trough trace. 2.  
449 Based on the relationship between  $D_{SO_4}$  and growth rate (expressed as  $\text{mm yr}^{-1}$  linear extension) the  
450 partition coefficient between drip water and speleothem calcite can be predicted for different  
451 speleothems beyond the period of contemporary cave monitoring. Assuming an essentially constant  
452 pre-industrial sulphate flux to the stalagmite,  $D_{SO_4}$  variability should therefore reveal changes in drip  
453 water pH and by implication the relative strength of cave ventilation and external temperature  
454 dynamics over a range of timescales. However, both of these linkages to climate rely on minimal  
455 upstream changes in drip water sulphate and carbonate concentration induced by prior calcite  
456 precipitation (PCP), (cf. Borsato et al., 2016). Where PCP is apparent, the associated removal of  
457 carbonate from the drip water will tend to cause the aqueous sulphate/carbonate to rise. If the  
458 calcium carbonate precipitation was stimulated by a winter fall in  $\text{CO}_2$  (rise in pH), the PCP effect will  
459 oppose the fall in speleothem sulphate that would otherwise be the hallmark of the seasonal  
460 change. PCP would therefore diminish the magnitude and duration of seasonal cycles in speleothem  
461 sulphate content. When the relationship between  $D_{SO_4}$  and speleothem growth rate is used to infer  
462 past changes in drip water pH, PCP would serve to disrupt this relationship. For the Ernesto cave  
463 system where PCP is of minimal significance, seasonal cycles in sulphate concentration and  
464 reconstructed values of  $D_{SO_4}$  can be used to infer changing environmental conditions as detailed  
465 above. However, when PCP plays a significant role in modifying drip water  $\text{SO}_4/\text{CO}_3$  content, other  
466 proxies of PCP (Mg/Ca and Sr/Ca in speleothem carbonate, Fairchild et al., 2000) need to be used to  
467 identify the extent of the process and the suitability of the sulphate record for environmental  
468 reconstruction. Consequently, when PCP can be deemed negligible or accounted for, both the pH

469 driver of sulphate incorporation and the universal relationship between  $D_{SO_4}$  and growth rate  
470 therefore raise the possibility of using speleothem sulphate content as a proxy for changing  
471 seasonality in different environmental settings. When used as part of a multi-proxy approach,  
472 sulphate thereby promises to enhance the resolving power of speleothem archives of environmental  
473 change.

474

## 475 **Conclusions**

476 Calcite grown under controlled laboratory conditions provides the first quantitative description of  
477 the controls on annual cycles in speleothem sulphate. pH is confirmed as the dominant variable  
478 controlling the overall abundance of sulphate incorporated into calcite. The efficiency of sulphate  
479 incorporation into calcite ( $D_{SO_4}$ ) is enhanced at high pH, high crystal growth rate and low sulphate  
480 concentrations in aqueous media. Increased  $D_{SO_4}$ , despite the lower sulphate ion abundance,  
481 probably reflects an increase in defect sites at calcite crystal surfaces associated with high levels of  
482 supersaturation, as well as bicarbonate competition at the calcite surface. In most cave  
483 environments, drip water pH is controlled by ventilation dynamics. Where cave ventilation is  
484 seasonal, the associated speleothem calcite will demonstrate a seasonality to sulphate  
485 incorporation. At the Obir and Ernesto caves, cave ventilation control of pH leads to characteristic  
486 summer peaks and winter lows in speleothem sulphate content. Increased crystal defects and  
487 limited bicarbonate competition associated with high levels of supersaturation during the winter  
488 season (low cave air  $pCO_2$ ), likely explain the greater efficiency of sulphate incorporation at this time  
489 of year despite a lower  $SO_4/CO_3$  ion abundance in drip waters. These same defect-rich crystallites are  
490 also responsible for the blurred transition in sulphur concentration between summer and winter  
491 seasons in the speleothem record. The experimental values of  $D_{SO_4}$  generated as a part of this study  
492 quantitatively reflect the incorporation of sulphate into contemporary speleothem calcite for  
493 stalagmites which have grown in a range of cave settings. Due to the universal applicability of the  
494 relationship between speleothem growth rate and  $D_{SO_4}$ , this opens the possibility of using  
495 speleothem records to reconstruct environmental drivers of sulphate partitioning, namely cave  
496 ventilation and external temperature dynamics across well-defined climatic changes where the  
497 effects of PCP are absent or can be accounted for.

498

## 499 **Acknowledgements**

500 The authors would like to thank the UK Natural Environment Research Council (NERC) for funding  
501 this work (Grant NE/C511805/1). Funding was also received from the European Synchrotron  
502 Radiation Facility (Experiment EC710) for the production of Figure 1, and from the Nuffield  
503 foundation (Grant URB/33218) for the financial support to Adam Hartland. The underlying data  
504 pertaining to the calcite growth experiments and the primary data associated with Tables 2-4 is  
505 available from <http://dx.doi.org/10.17635/lancaster/researchdata/xxx>. We are grateful for the kind  
506 permission from Dr. L. Fuller to use cave monitoring data from her PhD thesis (presented in Table 3).  
507 Thanks are also expressed to Dr's. K. Jarvis and K. Linge at the NERC ICP-MS facility, Kingston  
508 University for assistance with sulphur analysis in carbonate materials.

510 **References**

- 511 Andersson, M.P., Rodriguez-Blanco, J.D. and Stipp, S.L.S. (2016) Is bicarbonate stable in and on the  
512 calcite surface? *Geochimica et Cosmochimica Acta*, **176**, 198-205.
- 513 Asrat A., Baker A., Umer MM., Leng MJ., Van Calsteren., P. and Smith C. (2007) A high-resolution  
514 multi-proxy stalagmite record from Mechara, Southeastern Ethiopia: palaeohydrological  
515 implications for speleothem palaeoclimate reconstruction. *Journal of Quaternary Science*, **22**,  
516 53–63.
- 517 Asrat, A., Baker, A., Leng, M.J., Gunn, J. and Umer, M. (2008) Environmental monitoring in the  
518 Mechara caves, Southeastern Ethiopia: implications for speleothem palaeoclimate studies.  
519 *International Journal of Speleology* **37 (3)** 207-220
- 520 Badertscher, S., Borsato, A., Frisia, S., Cheng, H., Edwards, RL., Tüysüz, O. and Fleitmann, D. (2014)  
521 Speleothems as sensitive recorders of volcanic eruptions – the Bronze Age Minoan eruption  
522 recorded in a stalagmite from Turkey. *Earth and Planetary Science Letters*, **392**, 58-66.
- 523 Baker, A., Genty, D., Dreybodt, W., Barnes, W., Mockler, N and Grapes, J. (1998) Testing theoretically  
524 predicted stalagmite growth rate with recently annually laminated samples: Implications for past  
525 stalagmite deposition. *Geochimica et Cosmochimica Acta*, **62**, 393-404.
- 526 Baker, A., Mockler, N., Barnes, W. (1999) Fluorescence intensity variations of speleothem forming  
527 groundwaters: Implications for paleoclimate reconstruction. *Water Resources Research*, **35**, 407-  
528 413.
- 529 Baker, A., Asrat, A., Fairchild, I.J., Leng, M.J., Wynn, P.M., Bryant, C. Genty, D. and Umer, M. (2007)  
530 Analysis of the climate signal contained within  $\delta^{18}\text{O}$  and growth rate parameters in two Ethiopian  
531 stalagmites. *Geochimica et Cosmochimica Acta*. **71**, 2975-2988
- 532 Baker, A., Smith, C.L., Jex, C., Fairchild, I.J., Genty, D. and Fuller, L. (2008) Annually laminated  
533 speleothems: a review. *Int. J. Speleol.* **37**, 193-206.
- 534 Baker, A., Wilson, R., Fairchild, I. J., Franke, J., Spötl, C., Matthey, D., Trouet, V., and Fuller, L. 2011.  
535 High resolution  $\delta^{18}\text{O}$  and  $\delta^{13}\text{C}$  records from an annually laminated Scottish stalagmite and  
536 relationship with last millennium climate. *Global and Planetary Change*, **79**, 303-311.
- 537 Baker, A., Bradely, C., Phipps, S.J., Fischer, M., Fairchild, I.J., Fuller, L., Spötl, C. and Azcurra, C. (2012)  
538 Millennial-length forward models and pseudoproxies of stalagmite  $\delta^{18}\text{O}$ : an example from NW  
539 Scotland. *Climate of the Past*, **8**, 1153-1167.
- 540 Baker, A., Hellstrom, J.C., Kelley, B.F.J., Mariethoz, G. and Trouet, V. (2015) A composite annual-  
541 resolution stalagmite record of North Atlantic climate over the last three millennia. *Scientific*  
542 *Reports*, **5**, art. No. 10307.
- 543 Baldini, J. (2001) Morphological and dimensional linkage between recently deposited speleothems  
544 and drip water from Browns Folly Mine, Wiltshire, England. *Journal of Cave and Karst Studies* **63**:  
545 83-90.
- 546 Baldini, J.U.L, McDermott, F., Baker, A., Baldini, L.M., Matthey, D.P and Railsback., L.B. (2005) Biomass  
547 effects on stalagmite growth and isotope ratios: A 20<sup>th</sup> century analogue from Wiltshire, England.  
548 *Earth and Planetary Science Letters*, **240**, 486-494.
- 549 Baldini, J.U.L., McDermott, F. and Fairchild, I.J. (2006) Spatial variability in cave drip water  
550 hydrochemistry: Implications for stalagmite palaeoclimate records. *Chemical Geology*, **235**, 390-  
551 404
- 552 Baldini, J.U.L., McDermott, F., Hoffman D.L, Richards, D.A. and Clipson, N. (2008) Very high frequency  
553 and seasonal cave atmosphere  $\text{Pco}_2$  variability: Implications for stalagmite growth and oxygen  
554 isotope-based palaeoclimate records. *Earth and Planetary Science Letters*, **272 (1-2)** 118-129.
- 555 Bao, H.M., Fairchild, I.J., Wynn, P.M., Spötl, C. (2009) Stretching the envelope of past surface  
556 environments: Neoproterozoic glacial lakes from Svalbard. *Science*, 323 (5910), 119-122.
- 557 Bao, H.M., Lyons, J.R. and Zhou, C. 2008. Triple oxygen isotope evidence for elevated  $\text{CO}_2$  levels after  
558 a Neoproterozoic glaciation. *Nature*, **453**, 504-506.

559 Benn, D.I., Le Hir, G., Bao, H., Donnadiou, Y., Dumas, C., Fleming, E.J., Hambrey, M.J., McMillan, E.A.,  
560 Petronis, M.S., Ramstein, G., Stevenson, C.T.E., Wynn, P.M. and Fairchild, I.J. (2015) Orbitally Forced  
561 Ice Sheet Fluctuations in Snowball Earth. *Nature Geoscience*, **8**, 704-707.

562 Blyth, A.J., Asrat, A., Baker, A., Gulliver, P., Leng, M.J. and Genty, D. (2007) A new approach to  
563 detecting vegetation and land-use change using high-resolution lipid biomarker records in  
564 stalagmites. *Quaternary Research*, **68** (3) 314-324.

565 Borsato, A., Frisia, S., Fairchild, I.J., Somogyi, A. and Susini, J. (2007) Trace element distribution in  
566 annual stalagmite laminae mapped by micrometer resolution X-ray fluorescence: implications for  
567 incorporation of environmentally significant species. *Geochimica et Cosmochimica Acta*. **71**,  
568 1494-1512

569 Borsato, A., Frisia, S., Wynn, P., Fairchild, I.J. and Miorandi, R. (2015) Sulphate concentration in cave  
570 drip water and speleothems: long-term trends and overview of its significance as proxy of  
571 environmental processes and climate forcing. *Quat. Sci. Rev.*, **127**, 48-60.

572 Borsato, A., Johnston, V., Frisia, S., Miorandi, R., & Corradini, F. (2016). Temperature and altitudinal  
573 influence on karst drip water chemistry: implications for regional-scale palaeoclimate  
574 reconstructions from speleothems. *Geochimica et Cosmochimica Acta* **177**, 275–297.

575 Bottrell, S.H. and Newton, R.J. (2006) Reconstruction of changes in global sulphur cycling from  
576 marine sulphate isotopes. *Earth-Science Reviews*, **75**, 59-83.

577 Burdett J. W., Arthur M. A., and Richardson M. (1989) A Neogene seawater isotope age curve from  
578 calcareous pelagic microfossils. *Earth Planet. Sci. Lett.* **94**, 189–198.

579 Busenberg, E. and Plummer, L.N. (1985) Kinetic and thermodynamic factors controlling the  
580 distribution of  $\text{SO}_4^{2-}$  and  $\text{Na}^+$  in calcites and selected aragonites. *Geochim. Cosmochim. Acta* **49**,  
581 713-725.

582 Day, C. and Henderson, G.M. (2013) Controls on trace-element partitioning in cave-analogue calcite.  
583 *Geochim. Cosmochim. Acta*, **120**, 612-627.

584 Fairchild, I.J. Borsato, A., Tooth, A., Frisia, S., Hawkesworth, C.J., Huang, Y., McDermott, F. and Spiro,  
585 B. (2000) Controls on trace element (Mg-Sr) compositions of carbonate cave waters: implications  
586 for speleothem climatic records. *Chemical Geology*, **166**, 255-269.

587 Fairchild, I.J., Tuckwell, G.W., Baker, A and Tooth, A.F. (2006) Modelling of drip water hydrology and  
588 hydrogeochemistry in a weakly karstified aquifer (Bath, UK): Implications for climate change  
589 studies. *Journal of Hydrology*, **321**, 213-231.

590 Fairchild, I.J., Spötl, C., Frisia, S., Borsato, A., Susini, J., Wynn, P.M., Cauzid, J. and EIMF (2010)  
591 Petrology and geochemistry of annually laminated stalagmites from an Alpine cave (Obir,  
592 Austria): seasonal cave physiology. In: Pedley, H.M. & Rogerson, M. (eds) *Tufas and Speleothems:  
593 Unravelling the Microbial and Physical Controls*. Geol. Soc. Lond. Spec. Publ., **336**, 295–321.

594 Fairchild, I.J. and Baker, A. (2012) *Speleothem Science. From Process to Past Environment*. Wiley,  
595 Chichester.

596 Feng, J., Lee, Y.J., Reeder, R.J and Phillips, B.L. (2006) Observation of bicarbonate in calcite by NMR  
597 spectroscopy. *American Mineralogy*, **91**, 957-960.

598 Frisia S., Borsato, A., Fairchild, I. J. and McDermott, F. (2000) Calcite fabrics, growth mechanisms,  
599 and environments of formation in speleothems from the Italian alps and southwestern Ireland.  
600 *Journal of sedimentary research*, **70** (5) 1183-1196.

601 Frisia S., Borsato A., Fairchild I. J. and Susini J. (2005) Variations in atmospheric sulphate recorded in  
602 stalagmites by synchrotron micro XRF and XANES analyses. *Earth Plan. Sci. Lett.* **235**, 729-740.

603 Frisia, S., Borsato, A. & Susini, J. (2008) Synchrotron radiation applications to past volcanism archived  
604 in speleothems: An overview. *J. Volcanol. Geotherm. Res*, **177**, 96-100.

605 Frisia, S., Fairchild, I.J., Fohlmeister, J., Miorandi, R. Spötl, C. and Borsato, A. (2011) Carbon mass-  
606 balance modelling and carbon isotope exchange processes in dynamic caves. *Geochim.  
607 Cosmochim. Acta*, **75**, 380-400.

608 Fuller, L. (2006) High-resolution multiproxy geochemical Holocene climate records from 1000-year  
609 old Scottish stalagmites. *Ph.D thesis, University of Birmingham*.

610 Fuller, L., Baker, A., Fairchild, I.J., Spötl, C., Marca-Bell, A., Rowe, P. and Dennis, P.F. (2008) Isotope  
611 hydrology of dripwaters in a Scottish cave and implications for stalagmite palaeoclimate  
612 research. *Hydrology and Earth System Sciences*, **12** (4) 1065-1074

613 Hartland, A., Fairchild, I.J., Lead, J.R., Zhang, H. and Baalousha, M. (2011) Size, speciation and lability  
614 of NOM-metal complexes in hyperalkaline cave drip water. *Geochim. Cosmochim. Acta*, **75**, 7531-  
615 7577.

616 Hartland, A., Fairchild, I.J., Lead, J.R., Borsato, A., Baker, A., Frisia, S., Baalousha, M. (2012) From soil  
617 to cave: transport of trace metals by natural organic matter in karst drip waters. *Chem. Geol.*,  
618 **304**, 68-82.

619 Huang, Y. and Fairchild, I.J. (2001) Partitioning of Sr<sup>2+</sup> and Mg<sup>2+</sup> into calcite under karst-analogue  
620 experimental conditions. *Geochim. Cosmochim. Acta*, **65**, 47-62.

621 Hughes, S.G., Taylor, E.L., Wentzell, P.D., McCurdy, R.F. and Boss, R.K. (1994) Models of conductance  
622 measurement in quality assurance of water analysis. *Anal. Chem.* **66**, 830-835.

623 James, E.W., Banner, J.L. and Hardt, B. (2015) A global model for cave ventilation and seasonal bias in  
624 speleothem palaeoclimate records. *Geochemistry, Geophysics, Geosystems*, **16**, 1044-1051

625 Leito, I., Strauss, L., Koort, E. and Pihl, V. (2002) Estimation of uncertainty in routine pH  
626 measurement. *Accred. Qual. Assur.* **7**, 242-249

627 Lorens, R.B. (1981) Sr, Cd, Mn and Co distribution coefficients in calcite as a function of calcite  
628 precipitation rate. *Geochim. Cosmochim. Acta*, **45**, 553-561.

629 McDermott, F., Frisia, S., Huang, Y M, Longinelli, A, Spiro, B, Heaton, T H E, Hawkesworth, C J, Borsato,  
630 A, Keppens, E, Fairchild, I J, van der Borg, K, Verheyden, S and Selmo, E. (1999) Holocene climate  
631 variability in Europe: Evidence from delta O-18, textural and extension-rate variations in three  
632 speleothems. *Quaternary Science Reviews*, **18**, 1021-1038.

633 McIntyre, W . L. (1963) Trace element partition coefficients -- a review of theory and applications to  
634 geology. *Geochim. Cosmochim. Acta* **27**, 1029-1264.

635 Miorandi, R., Borsato, A., Frisia, S., Fairchild, I.J. & Richter, D.K. (2010) Epikarst hydrology and  
636 implications for stalagmite capture of climate changes at Grotta di Ernesto (N.E. Italy): results  
637 from long-term monitoring. *Hydrol. Proc.* **24**, 3101-3114.

638 Mucci, A. and Morse, J.W. (1983) The incorporation of Mg<sup>2+</sup> and Sr<sup>2+</sup> into calcite overgrowths –  
639 influences of growth rate and solution composition. *Geochimica et Cosmochimica Acta*, **47** (2)  
640 217-233.

641 Nagra, G., Treble, P.C., Anderson, M.S., Fairchild, I.J., Coleborn, K. and Baker, A. (2016) A post-wildfire  
642 response in cave dripwater chemistry. *Hydrology and Earth System Sciences*, **20**, 2745-2758.

643 Pingitore NE and Eastman MP. (1986) The co-precipitation of Sr<sup>2+</sup> with calcite at 25 and 1 atm.  
644 *Geochimica et Cosmochimica Acta*, **50**, 2195-2203

645 Pingitore, N.E., Meitzner, G. & Love, K.M. (1995) Identification of sulfate in natural carbonates by X-  
646 ray absorption spectroscopy. *Geochim. Cosmochim. Acta*, **59**, 2477-2483.

647 Plummer, L.N., Parkhurst, D & Kosiur, D.R. (1975) MIX2, a computer program for modeling chemical  
648 reactions in natural waters. *U.S. Geological Survey, Water Resources Investigations Report* **61**,  
649 75p.

650 Proctor, C.J., Baker, A., Barnes, W.L. and Gilmour, M. (2000) A thousand year speleothem proxy  
651 record of North Atlantic climate from Scotland. *Climate Dynamics*, **16**, 815-820.

652 Przybylinski, J.L. 1987. The role of bicarbonate ion in calcite scale formation. *Society of Petroleum*  
653 *Engineers*, **2**, 63-67.

654 Reeder, R.J., Lamble, G.M., Lee, J.F. and Staudt, W.J. (1994) Mechanism of SeO<sub>4</sub><sup>2-</sup> substitution in  
655 calcite: an EXAFS study. *Geochim. Cosmochim. Acta*, **58**, 5639-5646.

656 Rennie, VCF. and Turchyn, A. (2014) The preservation of δ<sup>34</sup>Sso4 and δ<sup>18</sup>Oso4 in carbonate associated  
657 sulfate during marine diagenesis: A 25Myr test case using marine sediments. *Earth and Planetary*  
658 *Science Letters*, **395**, 13-23.

- 659 Sherwin, C.M and Baldini J.U.L. (2011) Cave air and hydrological controls on prior calcite  
660 precipitation and stalagmite growth rates: Implications for palaeoclimate reconstructions using  
661 speleothems. *Geochimica et Cosmochimica Acta*, **75 (14)** 3915-3929.
- 662 Smith, C.L., Fairchild, I.J., Spötl, C., Frisia, S., Borsato, A., Moreton, S.G. and Wynn, P.M. (2009)  
663 Chronology-building using objective identification of annual signals in trace element profiles of  
664 stalagmites. *Quat. Geochron.* **4**, 11-21.
- 665 Spötl., C., Fairchild I. J. and Tooth A.F. (2005) Cave air control on drip water geochemistry, Obir Caves  
666 (Austria): Implications for speleothem deposition in dynamically ventilated caves. *Geochim.*  
667 *Cosmochim. Acta* **69**, 2451-2468.
- 668 Staudt, W.J., Reeder, R., Schoonen, MA. (1994) Surface structural controls on compositional zoning  
669 of  $\text{SO}_4^{2-}$  and  $\text{SeO}_4^{2-}$  in synthetic calcite single crystals. *Geochimica et Cosmochimica Acta*. **58 (9)**  
670 2087-2098.
- 671 Tooth, A.F. and Fairchild, I.J. (2003) Soil and karst aquifer hydrological controls on the geochemical  
672 evolution of speleothem forming drip waters, Crag Cave, southwest Ireland. *Journal of*  
673 *Hydrology*, **273**, 51-68.
- 674 Treble, PC., Fairchild, I.J., Baker, A., Meredith, KT., Anderson, MS., Salmon, SU., Bradely, C., Wynn,  
675 PM., Hankin, S., Wood, A. and McGuire, E. (2016) Roles of forest bioproductivity, transpiration,  
676 and fire in a nine-year record of cave dripwater chemistry from southwest Australia. *Geochimica*  
677 *et Cosmochimica Acta*, **184**, 132-150.
- 678 Uchida, S., Kurisaki, K., Ishihara, Y., Haraguchi, S., Yamanaka, T., Noto, M., Yoshimura, K. (2013)  
679 Anthropogenic impact records of nature for past hundred years extracted from stalagmites in  
680 caves found in the Nanatsugama Sandstone Formation, Saikai, Southwestern Japan. *Chemical*  
681 *Geology* **347**, 59-68.
- 682 Uchikawa, J., Harper, DT., Penman, DE., Zachos, JC., Zeebe, RE. (2017) Influence of solution  
683 chemistry on the boron content in inorganic calcite grown in artificial sweater. *Geochimica et*  
684 *Cosmochimica Acta*, 218, 291-307.
- 685 van der Weijden RD., van der Heijden RD., Witkamp GJ., and van Rosmalen GM (1997) The influence  
686 of total calcium and total carbonate on the growth rate of calcite. *Journal of crystal growth*, 171,  
687 190-196.
- 688 van der Weijden, CH. and van der Weijden RD. (2014) Calcite growth: rate dependence on  
689 saturation, on ratios of dissolved calcium and (bi)carbonate and on their complexes. *Journal of*  
690 *crystal growth*, 394, 137-144.
- 691 Wynn, P.M., Fairchild, I.J., Baker, A., Baldini, J.U.L. and McDermott, F. (2008) Isotopic archives of  
692 sulphate in speleothems. *Geochim. Cosmochim. Acta* **72**, 2465-2477.
- 693 Wynn, P. M., Fairchild, I. J., Frisia, S., Spötl, C., Baker, A., Borsato, A. and EIMF (2010) High-resolution  
694 sulphur isotope analysis of speleothem carbonate by secondary ionization mass spectrometry.  
695 *Chem. Geol.* **271**, 101-107.
- 696 Wynn, P.M., Borsato, A., Baker, A., Frisia, S., Miorandi, R. & Fairchild, I.J. (2013) Biogeochemical  
697 cycling of sulphur in karst and transfer into speleothem archives at Grotta di Ernesto, Italy.  
698 *Biogeochemistry* **114**, 255-267.
- 699 Wynn, P.M., Fairchild, I.J., Spötl, C., Hartland, A. Matthey, D., Fayard, B. and Cotte, M. (2014)  
700 Synchrotron X-ray distinction of seasonal hydrological and temperature patterns in speleothem  
701 carbonate. *Environ. Chem*, **11**, 28-36.

704 **Figure captions**

705 **Figure 1:** Micro X-ray fluorescence mapping of speleothem sulphate and zinc content in sample  
706 Obi84. Concentrations are relative and denoted according to colour temperature scale with deep  
707 blue representing the lowest and yellow the highest concentrations in both sulphate and zinc maps.  
708 Autumnal peaks in colloiddally transported elements (shown here as a Zn trace) are clearly  
709 demarcated, allowing attribution of summer high and winter low concentrations of sulphur within  
710 an annual cycle. In contrast to the clear pulses of colloidal elements recorded within the speleothem  
711 calcite, the sulphate content poorly defines the seasonal switch in ventilation regime which should  
712 cause a rapid change in drip water pH and sulphate incorporation. Figure adapted from Wynn et al.,  
713 2014.

714 **Figure 2:** Experimental conditions of pH and calcite saturation for each growth chamber depicting  
715 conditions prior to calcite precipitation and throughout the experiment duration. The weighted  
716 mean conditions of each experiment are plotted, and dashed lines represent the locus of possible  
717 original experimental conditions based on growth media composition. The calcite saturation index  
718 ( $\Omega$ ) is calculated as  $\Omega = \log$  ionic activity product over solubility product.

719 **Figure 3:** Experimental progress of C1N1-8.0 depicting the drop in pH and EC between weekly  
720 interventions and solution restoration. The incremental rise in EC throughout the duration of the  
721 study reflects the use of a mixed restoration solution of 0.1M  $\text{CaCl}_2$  and 0.2M  $\text{NaHCO}_3$  to replenish  
722 the  $\text{Ca}^{2+}$ ,  $\text{HCO}_3^-$  and  $\text{CO}_3^{2-}$  ions in solution, leading to accumulation of excess NaCl in solution.

723 **Figure 4:** The pH-dependence of sulphate incorporation into calcite. **a:** Concentrations of sulphate  
724 incorporated into calcite demonstrate a negative relationship whereby the increasing abundance of  
725 carbonate ions at high pH limits the availability of sulphate in the calcite. The slope of the  
726 relationship is statistically significant for high (20 ppm) concentrations of sulphate in solution  
727 (ANOVA f-test,  $p=0.044$ ), but statistically indistinguishable for low (2 ppm) concentration  
728 experiments. **b:** A positive relationship between  $D_{\text{so}_4}$  and pH demonstrates a greater efficiency of  
729 incorporation under growth media conditions of high pH and low sulphate concentration, despite  
730 the lower abundance of sulphate ions in solution relative to carbonate (ANOVA f-test,  $p<0.02$  for  
731 high (20 ppm) and  $p=0.05$  for low (2 ppm) experimental series).

732 **Figure 5:** The growth rate dependence of sulphate incorporation into calcite based on  $D_{\text{so}_4}$ . At  
733 constant pH, a greater efficiency of sulphate incorporation is implied at faster rates of growth.  
734 Multiple linear regression demonstrates significance at the 0.05 level for both **a:** high (20 ppm)  
735 sulphate experiments ( $D_{\text{so}_4} = -49.85 + 29.06 \text{ growth rate} + 6.90 \text{ pH}$ ;  $r^2 = 0.95$ ), and **b;** low (2 ppm)  
736 sulphate experiments ( $D_{\text{so}_4} = -336.17 + 61.11 \text{ growth rate} + 44.47 \text{ pH}$  ( $r^2 = 0.90$ )). Low sulphur  
737 experiments demonstrate greater efficiency of sulphate incorporation. Data points of constant pH  
738 are visually linked by solid black lines. Speleothems from Ernesto and Obir caves are plotted in figure  
739 5b including dripwater pH values for comparison to experimental data.

740 **Figure 6.** SEM images of product calcite crystals showing the presence of defect sites (visible as  
741 stepped crystal faces) grown across a range of saturation indices and pH values. Images shown relate  
742 to experimental products from (a) incubation C1N1 at pH 8.6 for 20 ppm aqueous sulphate  
743 concentration, (b) incubation C1N1 at pH 8.6 for 2 ppm aqueous sulphate concentration, (c)  
744 incubation C1N1 at pH 8.3 for 2 ppm aqueous sulphate, and (d) incubation C05N05 at pH 8.3 for 2

745 ppm aqueous sulphate concentration. Further information on experimental conditions associated  
746 with each incubation are available through Table 1.

747 **Figure 7:** The growth rate dependence of sulphate incorporation into calcite. At constant pH, a  
748 greater quantity of sulphate is incorporated at faster rates of growth. Multiple linear regression  
749 demonstrates significance at the 0.05 level for **a**: high (20 ppm) sulphate experiments ( $S$  in calcite =  
750  $1828.89 + 201.45 \text{ growth rate} - 190.75 \text{ pH}$ ;  $r^2 = 0.790$ ), and no statistical significance at **b**; low (2  
751 ppm) sulphate experiments.

752

753 **Figure 8:** The relationship between growth rate and partition coefficient depicted as a linear  
754 expression relating  $\text{LOG}(D)$  to  $\text{LOG}(R)$ . Data obtained from Busenberg and Plummer (1985) where  
755 sulphate concentrations range between 100 to 10,000 ppm in solution (ANOVA f-test,  $p=9.0 \times 10^{-13}$ ),  
756 and this study for high (20 ppm, ANOVA f-test  $p=0.00071$ ) and low (2 ppm, ANOVA f-test  $p=0.03$ )  
757 sulphate experiments.

758

#### 759 **Supplementary figure captions**

760 **Figure S1:** Experimental conditions of  $\text{PCO}_2$  and calcite saturation for each growth chamber depicting  
761 conditions prior to calcite precipitation and throughout the experiment duration. The weighted  
762 mean conditions of each experiment are plotted, and dashed lines represent the locus of possible  
763 original experimental conditions based on growth media composition. The calcite saturation index  
764 ( $\Omega$ ) is calculated as  $\Omega = \log$  ionic activity product over solubility product.

765 **Figure S2:** Change in Ca composition within each growth chamber experiment calculated by the fall  
766 in both EC and pH. Deviation from the 1:1 line is due to relatively poor instrumental precision in  
767 conductivity determination relative to incremental changes in solution composition. Conductivity  
768 meter WTW Multi 340i, Tetracon 325 measuring cell with manufacturers' precision of +/- 0.5 % of  
769 sample value.

770 **Figure S3:** Growth rate calculated as rates of linear extension and compared to experimental results  
771 from Mucci and Morse (1983).

772

#### 773 **Table captions:**

774 **Table 1:** Results from growth chamber experiments detailing experimental conditions and calculated  
775 partition coefficients.

776 **Table 2:** Seasonal partition coefficients between cave waters and speleothem calcite at the Obir and  
777 Ernesto cave systems.

778 **Table 3:** Calculated partition coefficients between cave waters and speleothem calcite at a range of  
779 cave systems, demonstrating the universal applicability of experimentally determined partition  
780 coefficient  $D_{\text{so}}$ . All data prefixed a-g are referenced through Table 4.

781 **Table 4:** Speleothem sample details and data sources associated with cave sites presented in Table  
782 3.

783

784

785

786

787

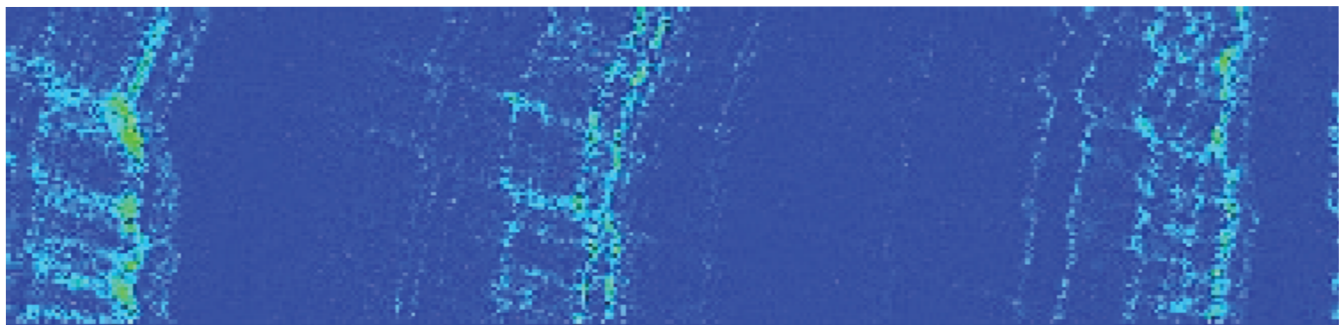
Growth direction

Autumn  
1977

Autumn  
1978

Autumn  
1979

Zinc



Sulphate



0

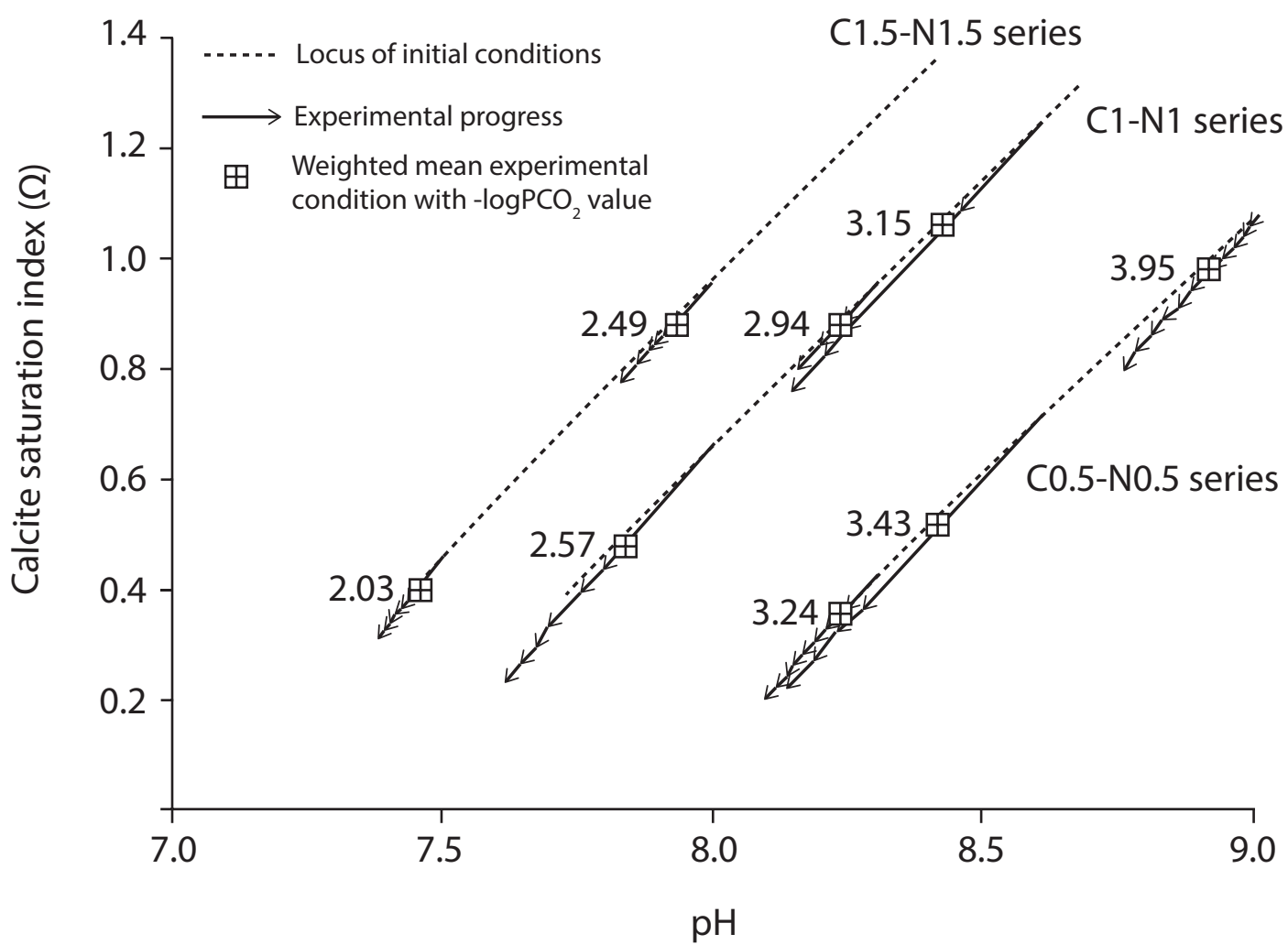
100

200

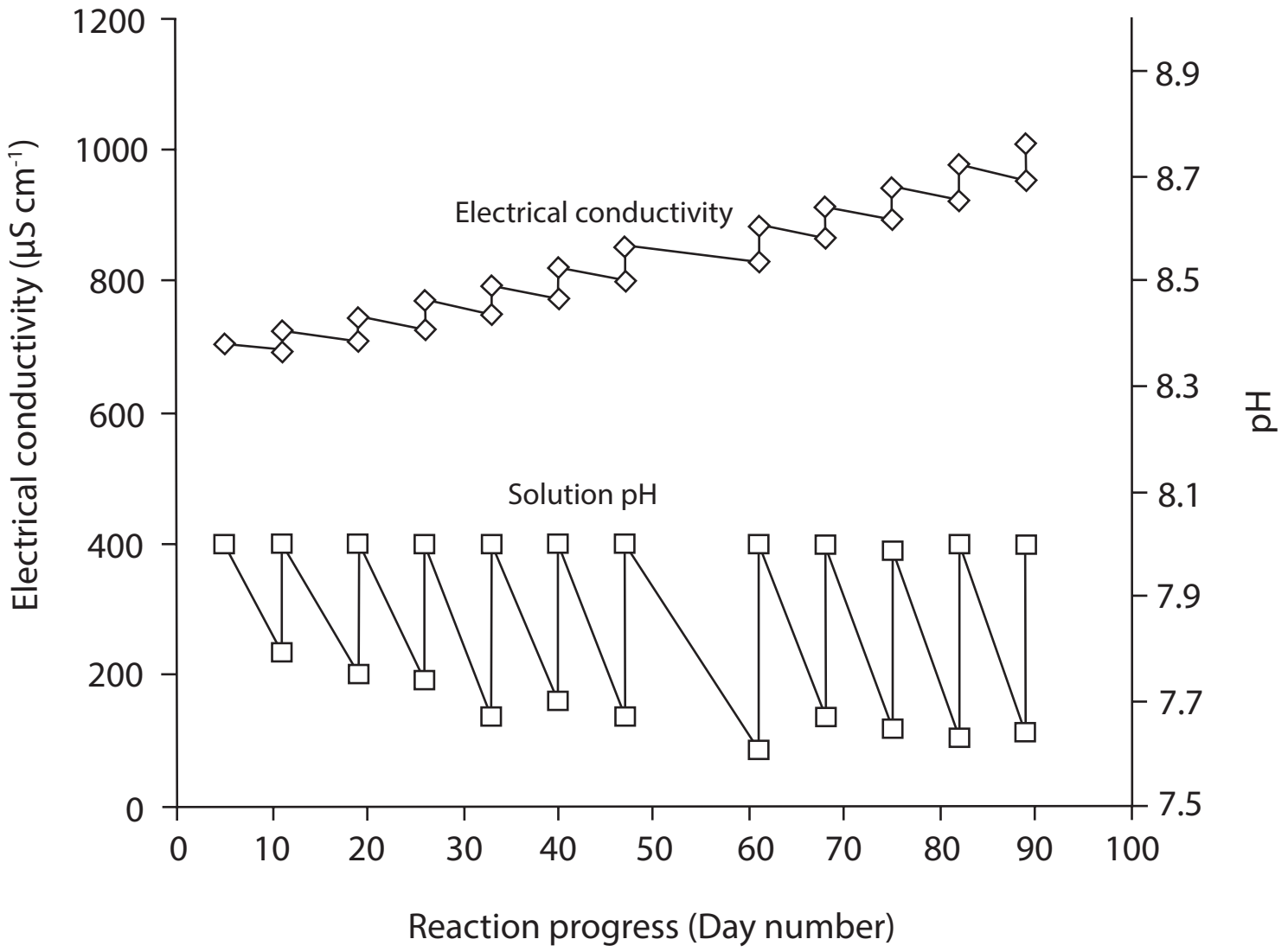
300

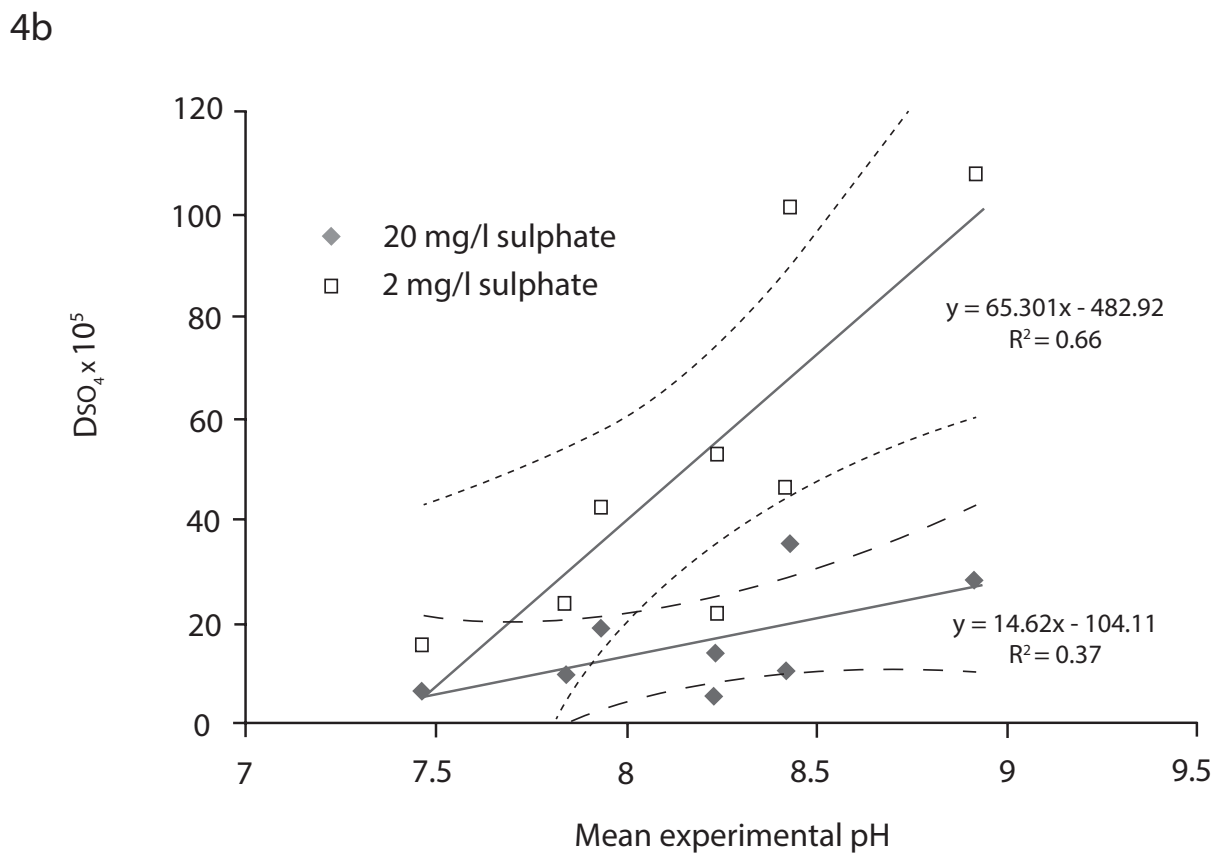
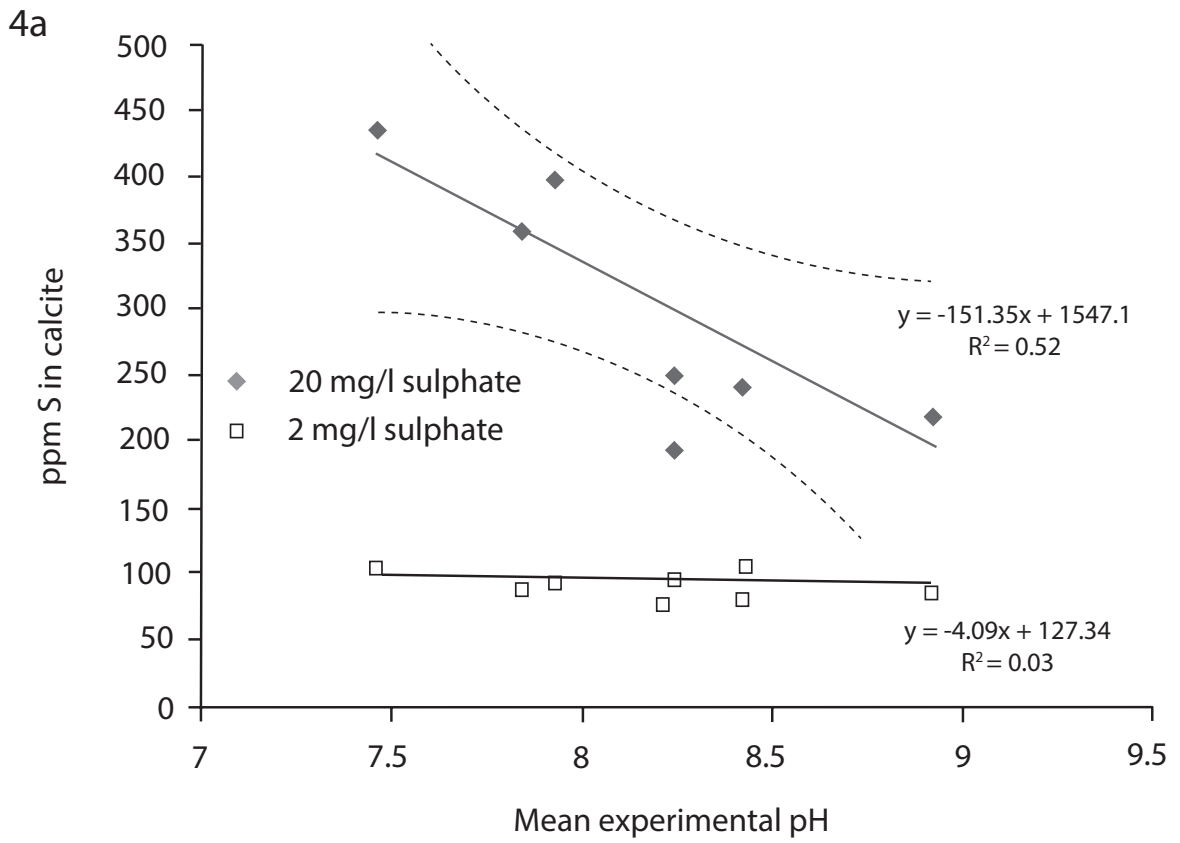
$\mu\text{m}$  along transect

Fig. 2

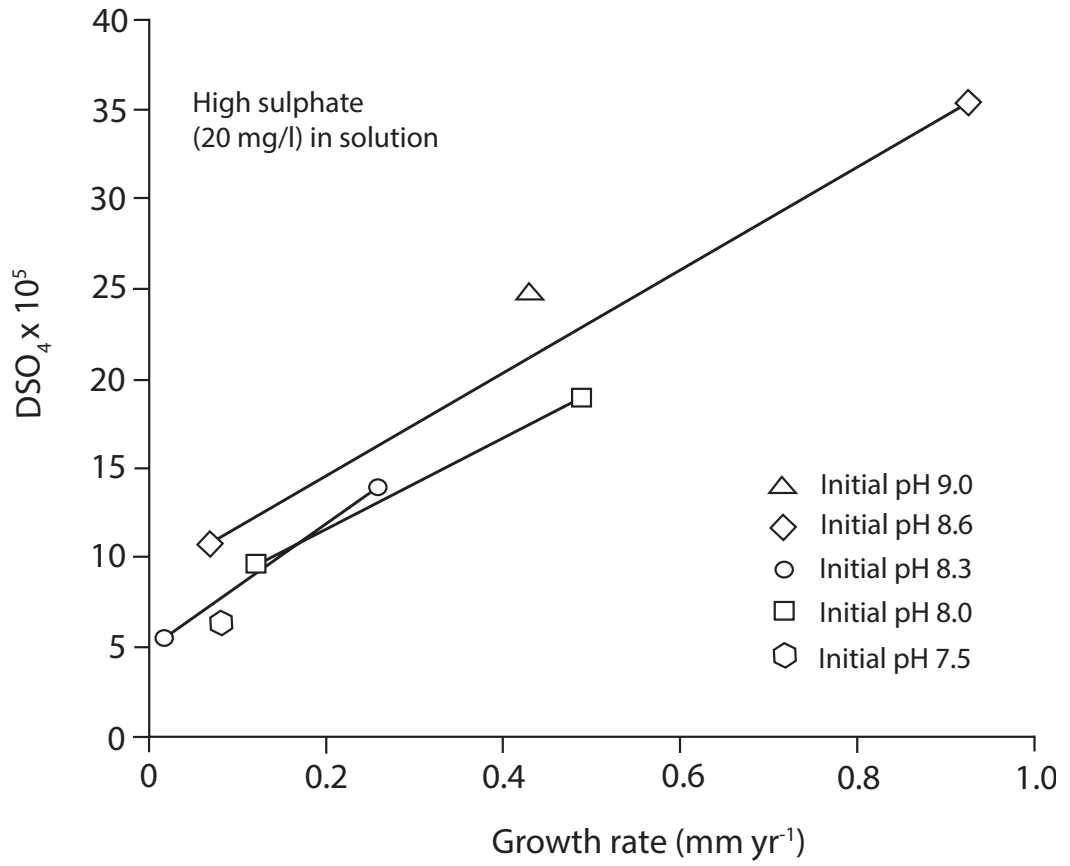


3.





5a



5b

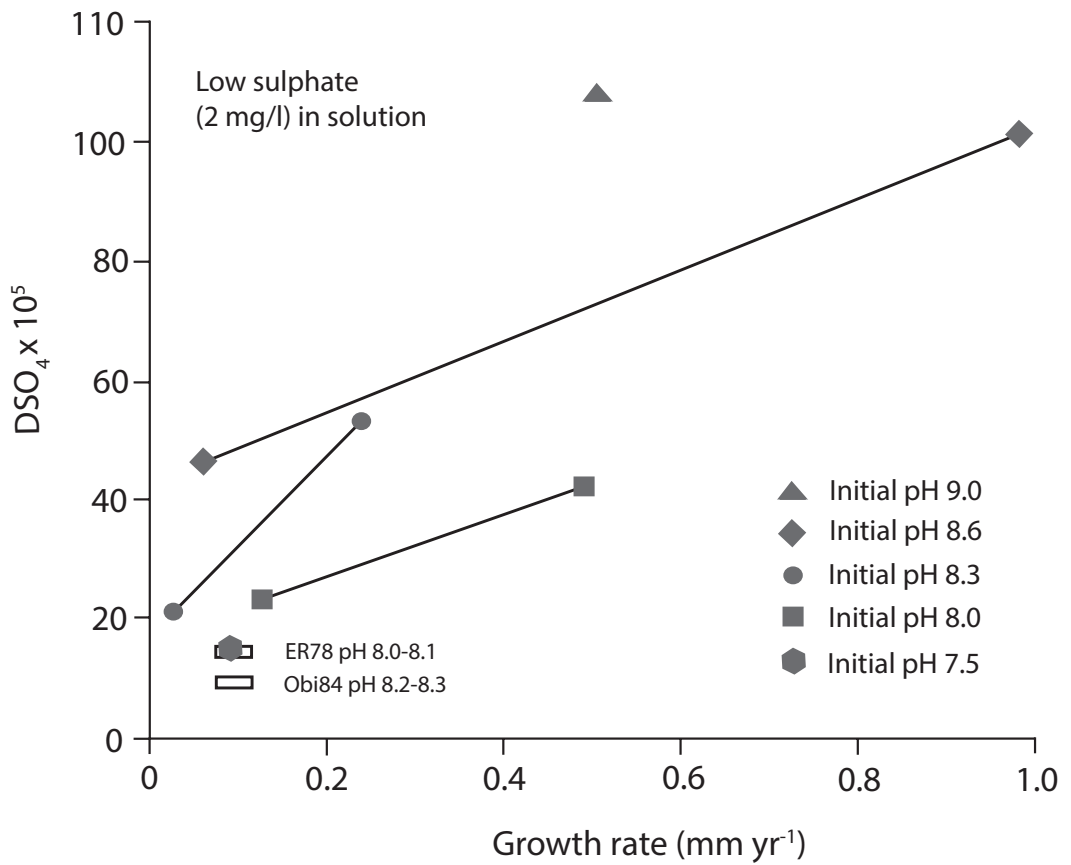
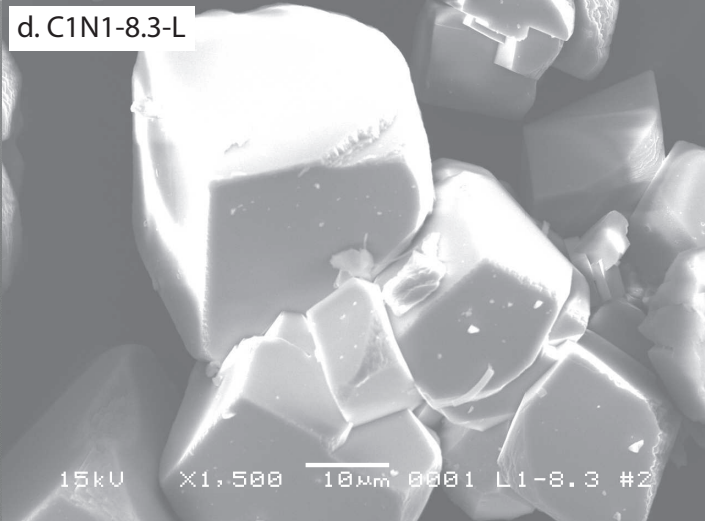
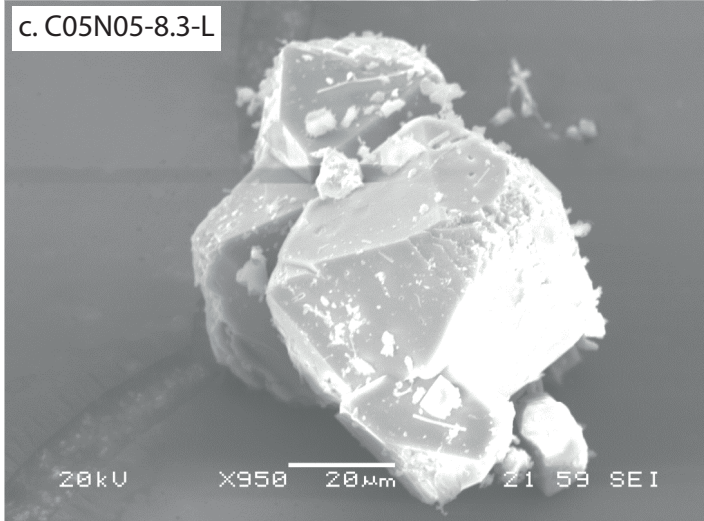
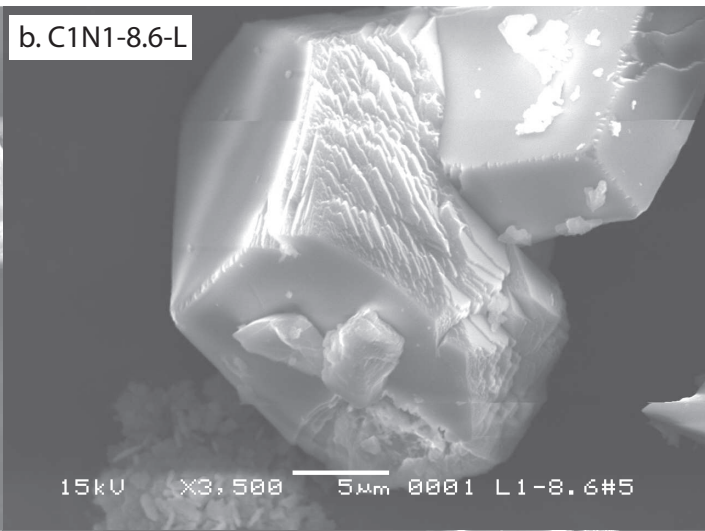
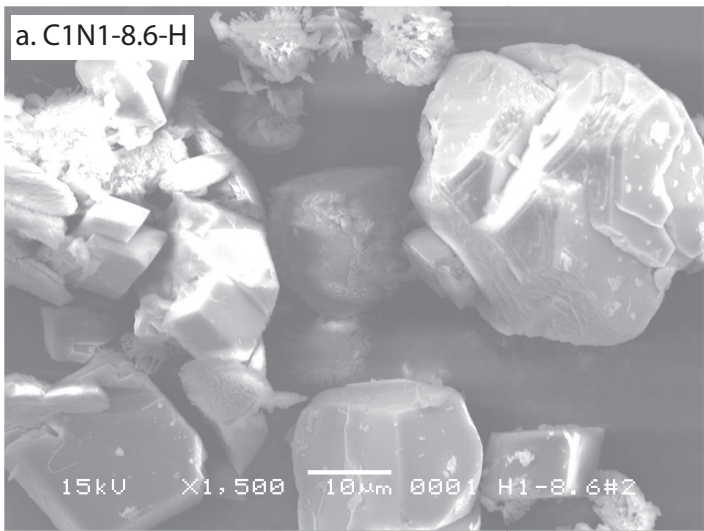
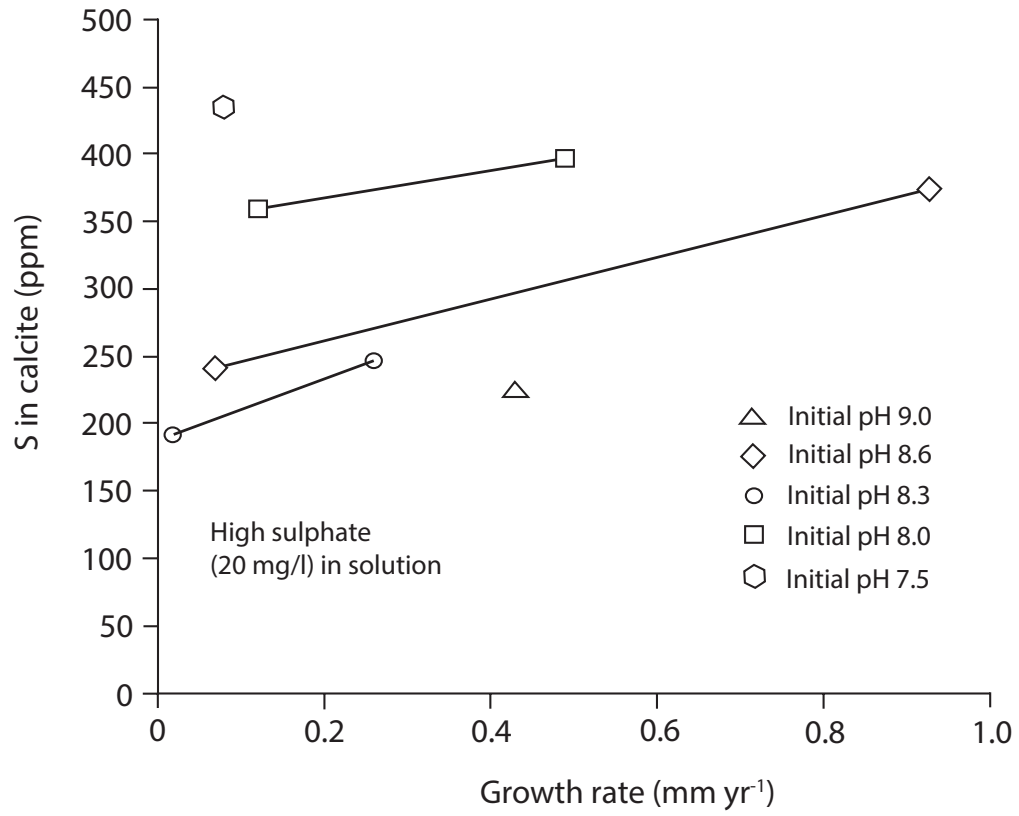


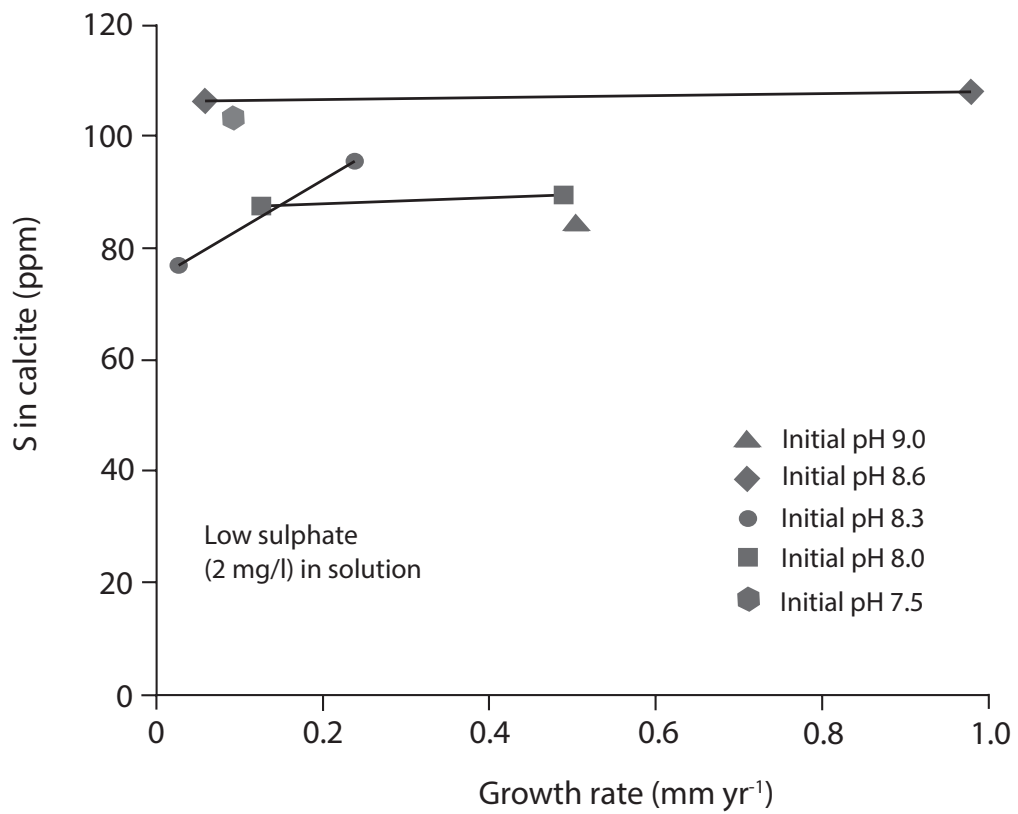
Figure 6



7a



7b



8.

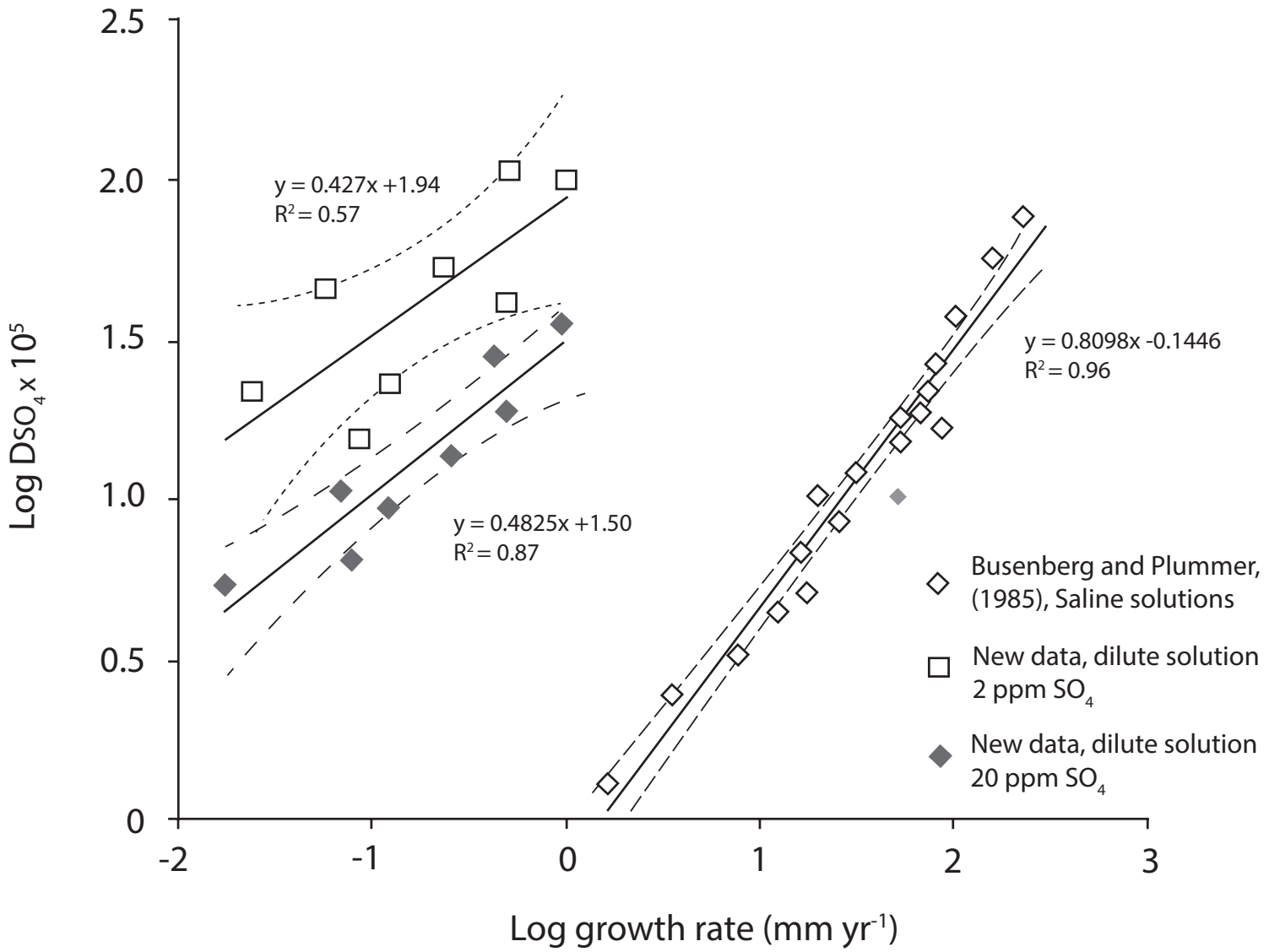


Table 1

Experiment number	pH <sup>a</sup>	Ω <sup>b</sup>	CO <sub>3</sub> (aq) (μM) <sup>c</sup>	HCO <sub>3</sub> (μM) <sup>d</sup>	νCO <sub>3</sub> <sup>e</sup>	νHCO <sub>3</sub> <sup>f</sup>	SO <sub>4</sub> (aq) (μM) <sup>g</sup>	SO <sub>4</sub> /CO <sub>3</sub> (aq) (M)	SO <sub>4</sub> (mM) calcite <sup>h</sup>	SO <sub>4</sub> /CO <sub>3</sub> calcite × 10 <sup>4</sup>	D <sub>SO4</sub> × 10 <sup>5</sup>	LOG D <sub>SO4</sub> × 10 <sup>5</sup>	Growth rate (mm yr <sup>-1</sup> )	LOG Growth rate (mm yr <sup>-1</sup> )
<b>High aqueous sulphate (20 mg/l)</b>														
C0.5N0.5 - 9.0	8.92 (8.78 - 9.0)	0.97 (0.79-1.07)	85.7 (60.5-103)	1665 (1647-1674)	0.755	0.93	208.2 (206.5-209.9)	2.43 (2.04-4.68)	6.8 (6.1-7.5)	6.8 (6.1-7.5)	28.1 (18.0-36.9)	1.45 (1.26-1.57)	0.43	-0.37
C1N1 - 8.6	8.43 (8.14 - 8.6)	1.05 (0.76-1.24)	63.1 (29.7-91.9)	3410 (3329-3470)	0.685	0.91	208.2 (206.5-209.9)	3.30 (2.28-11.3)	11.7 (10.7-12.6)	11.7 (10.7-12.6)	35.4 (15.4-55.3)	1.55 (1.19-1.74)	0.93	-0.03
C0.5N0.5 - 8.6	8.42 (8.17 - 8.6)	0.57 (0.31-0.71)	29.4 (14.3-42.4)	1703 (1675-1727)	0.76	0.93	208.2 (206.5-209.9)	7.08 (4.95-19.05)	7.5 (6.9-8.2)	7.5 (6.9-8.2)	10.65 (4.78-16.5)	1.03 (0.68-1.21)	0.07	-1.16
C1N1 - 8.3	8.24 (8.15 - 8.3)	0.87 (0.79-0.95)	37.1 (28.1-46.1)	3450 (3431-3470)	0.685	0.91	208.2 (206.5-209.9)	5.61 (4.55-11.0)	7.8 (7.0-8.5)	7.8 (7.0-8.5)	13.83 (9.55-18.7)	1.14 (0.98-1.27)	0.26	-0.59
C0.5N0.5 - 8.3	8.24 (8.13 - 8.3)	0.34 (0.23-0.42)	18.8 (14.4-21.3)	1720 (1710-1730)	0.76	0.93	208.2 (206.5-209.9)	11.07 (9.85-20.9)	6.0 (5.5-6.5)	6.0 (5.5-6.5)	5.4 (3.82-6.60)	0.73 (0.58-0.82)	0.02	-1.76
C1N1 - 8.0	7.84 (7.64 - 8.0)	0.5 (0.28-0.66)	17.7 (9.05-22.9)	3376 (3254-3450)	0.685	0.91	208.2 (206.5-209.9)	11.8 (9.16-35.8)	11.2 (10.4-12.1)	11.2 (10.4-12.1)	9.53 (4.53-13.2)	0.98 (0.66-1.12)	0.12	-0.92
C1.5N1.5 - 8.0	7.93 (7.81 - 8.0)	0.89 (0.75-0.96)	31.6 (23.8-36.0)	5120 (5020-5170)	0.64	0.89	208.2 (206.5-209.9)	6.6 (5.8-16.8)	12.4 (11.4-13.4)	12.4 (11.4-13.4)	18.8 (13.14-23.0)	1.28 (1.12-1.36)	0.49	-0.31
C1.5N1.5 - 7.5	7.46 (7.42 - 7.5)	0.4 (0.32-0.45)	9.89 (8.89-10.9)	4890 (4830-4950)	0.64	0.89	208.2 (206.5-209.9)	21.1 (19.3-41.3)	13.6 (12.6-14.6)	13.6 (12.6-14.6)	6.46 (5.40-7.60)	0.81 (0.73-0.88)	0.08	-1.10
<b>Low aqueous sulphate (2 mg/l)</b>														
C0.5N0.5 - 9.0	8.92 (8.78 - 9.0)	0.97 (0.79-1.07)	85.7 (60.5-103)	1665 (1647-1674)	0.755	0.93	20.8 (20.4-21.2)	0.24 (0.21-0.46)	2.6 (2.4-2.9)	2.63 (2.38-2.88)	108 (70.7-140)	2.03 (1.85-2.14)	0.51	-0.30
C1N1 - 8.6	8.43 (8.14 - 8.6)	1.05 (0.76-1.24)	63.1 (29.7-91.9)	3410 (3329-3470)	0.685	0.91	20.8 (20.4-21.2)	0.33 (0.23-1.12)	3.4 (3.1-3.6)	3.35 (3.07-3.64)	102 (44.6-157)	2.01 (1.65-2.20)	0.98	-0.01
C0.5N0.5 - 8.6	8.42 (8.16 - 8.6)	0.57 (0.31-0.71)	29.4 (13.7-42.4)	1703 (1674-1727)	0.755	0.93	20.8 (20.4-21.2)	0.71 (0.50-1.93)	3.3 (3.0-3.6)	3.29 (3.01-3.58)	46.5 (20.2-71.4)	1.67 (1.31-1.85)	0.06	-1.24
C1N1 - 8.3	8.24 (8.18 - 8.3)	0.87 (0.79-0.95)	37.1 (32.6-46.1)	3450 (3442-3470)	0.685	0.91	20.8 (20.4-21.2)	0.56 (0.46-1.01)	3.0 (2.7-3.3)	2.99 (2.67-3.31)	53.2 (42.6-71.9)	1.73 (1.63-1.86)	0.24	-0.63
C0.5N0.5 - 8.3	8.22 (8.08 - 8.3)	0.34 (0.23-0.42)	18.8 (13.0-21.3)	1720 (1700-1730)	0.755	0.93	20.8 (20.4-21.2)	1.11 (1.00-2.32)	2.4 (2.2-2.6)	2.41 (2.21-2.62)	21.8 (14.1-26.2)	1.34 (1.15-1.42)	0.02	-1.63
C1N1 - 8.0	7.84 (7.61 - 8.0)	0.5 (0.28-0.66)	17.7 (7.86-22.9)	3376 (3236-3450)	0.685	0.91	20.8 (20.4-21.2)	1.18 (0.93-3.79)	2.7 (2.5-3.0)	2.74 (2.53-2.95)	23.3 (9.73-31.9)	1.37 (0.99-1.5)	0.12	-0.91
C1.5N1.5 - 8.0	7.93 (7.81 - 8.0)	0.89 (0.75-0.96)	31.6 (23.8-36.0)	5120 (5020-5170)	0.64	0.89	20.8 (20.4-21.2)	0.66 (0.59-1.66)	2.8 (2.6-3.1)	2.80 (2.55-3.05)	42.4 (29.7-51.7)	1.63 (1.47-1.71)	0.49	-0.31
C1.5N1.5 - 7.5	7.46 (7.38 - 7.5)	0.4 (0.32-0.45)	9.89 (7.91-10.9)	4890 (4770-4950)	0.64	0.89	20.8 (20.4-21.2)	2.11 (1.95-4.51)	3.2 (3.0-3.5)	3.23 (2.98-3.48)	15.3 (11.6-17.9)	1.19 (1.06-1.25)	0.09	-1.07

Tabulated data are mean values, with the range associated with each parameter presented in parentheses. <sup>a-d</sup> Mean values are weighted according to the mass of calcium carbonate precipitated in each experiment. The range represents the spread of values in each measured data set. <sup>e-f</sup> Activity coefficients for  $\text{HCO}_3^-$  and  $\text{CO}_3^{2-}$  in solution were determined by PHREEQE and used to calculate both carbonate and bicarbonate ion concentration from the second dissociation constant for carbonic acid. <sup>g</sup> The range of aqueous sulphate concentrations reflects the maximum systematic error associated with pipetting. <sup>h</sup> The range of values associated with the sulphate content of product calcite are calculated based on an instrumental precision of 7.5% RSD from replicate analyses.  $\Omega = \log$  ionic activity product over solubility product.

Table 2

Cave water sample	Dripwater pH <sup>a</sup>	Dripwater CO <sub>3</sub> (μM) <sup>b</sup>	Dripwater HCO <sub>3</sub> (mM) <sup>c</sup>	Dripwater SO <sub>4</sub> (μM) <sup>d</sup>	Dripwater SO <sub>4</sub> /CO <sub>3</sub>	SO <sub>4</sub> (mM) in coeval speleothem calcite <sup>e</sup>	SO <sub>4</sub> /CO <sub>3</sub> Speleothem calcite X 10 <sup>4</sup>	D <sub>SO4</sub> x 10 <sup>5</sup> <sup>f</sup>	Speleothem growth rate (LOG mm/yr)	Expected D <sub>SO4</sub> x 10 <sup>5</sup> <sup>g</sup>
Obir cave*										
Winter average	8.30 (8.17 – 8.38)	40.8 (30.9 – 53.3)	3.0 (2.8 - 3.2)	46.9 (46.9 – 46.9)	1.2 (0.9 – 1.5)	1.3 (1.2 – 1.4)	1.3 (1.2 – 1.4)	11.1 (7.8 – 15.6)	-0.89	11.7 – 36.6
Summer average	8.15 (8.07 – 8.23)	29.7 (24.9 – 33.4)	3.2 (3.0 – 3.2)	46.9 (46.9 – 46.9)	1.6 (1.4 – 1.9)	1.4 (1.3 – 1.5)	1.4 (1.3 – 1.5)	9.0 (6.9 – 10.8)	-1.15	8.7 – 28.3
Ernesto Cave**										
Winter average	8.14 (7.94 – 8.33)	25.3 (12.5 – 41.0)	2.5 (2.15 - 2.88)	69.1 (65.7 – 71.0)	2.7 (1.7 – 5.3)	4.2 (3.9 – 4.5)	4.2 (3.9 – 4.5)	15.4 (7.4 – 26.1)	-0.89	11.7 – 36.6
Summer average	8.02 (7.84 – 8.14)	18.8 (12.7 – 27.4)	2.7 (2.14 – 3.03)	70.5 (65.3 – 72.6)	3.8 (2.7 – 5.1)	5.6 (5.2 – 6.0)	5.6 (5.2 – 6.0)	14.9 (10.0 – 22.6)	-1.15	8.7 – 28.3

Tabulated data are mean values, with the range associated with each parameter presented in parentheses. <sup>a-d</sup> Range represents the spread of values in each measured data set. <sup>e</sup> The range of values associated with the sulphate content of speleothem calcite are calculated based on an instrumental precision of 7.5% RSD from replicate analyses. <sup>f</sup> The range in D<sub>SO<sub>4</sub></sub> x 10<sup>5</sup> is calculated based on measured environmental parameters, including 7.5% RSD from <sup>e</sup> instrumental precision. <sup>g</sup> The range in expected D<sub>SO<sub>4</sub></sub> is calculated from the experimental data on sulphate partitioning extrapolated to appropriate growth rates (Figure 8) at low (2 ppm) and high (20 ppm) aqueous sulphate concentrations. Seasonal differences in D<sub>SO<sub>4</sub></sub> x 10<sup>5</sup> are statistically significant (p = 0.045, Mann Whitney U-test) at Obir cave, although at Ernesto cave D<sub>SO<sub>4</sub></sub> values are statistically indistinguishable between summer and winter seasons.

\*Obir cave waters represent average values for both summer and winter seasons throughout 2002-2004. Coeval speleothem calcite for this site represents the year 2000.

\*\*Ernesto cave waters represent average values for both summer and winter seasons throughout 1996-1997. Coeval speleothem calcite for this site represents the year 1996.



Table 3

Speleothem sample	Drip water pH <sup>a</sup>	Drip water CO <sub>3</sub> (μM) <sup>b</sup>	Dripwater HCO <sub>3</sub> (mM) <sup>c</sup>	Drip water SO <sub>4</sub> (μM) <sup>d</sup>	Drip water SO <sub>4</sub> /CO <sub>3</sub>	SO <sub>4</sub> (mM) in speleothem calcite <sup>e</sup>	SO <sub>4</sub> /CO <sub>3</sub> speleothem calcite x 10 <sup>4</sup>	D <sub>SO4</sub> x 10 <sup>5f</sup>	Speleothem growth rate (LOG mm/yr) <sup>g</sup>	Expected D <sub>SO4</sub> x 10 <sup>5h</sup>
ASFA 3	7.81 (7.47-8.15)	30.3 (5.9-100.9)	7.0 (3.2-10.7)	115.6 (112.1-125.1)	3.8 (19.1-1.2)	5.0 (4.6-5.3)	5.0 (4.6-5.3)	13.0 (2.4-43.1)	-0.52	14.4-44.2
MERC-1	7.81 (7.47-8.15)	24.7 (2.7-100.2)	6.2 (1.5-10.7)	31.3 (9.3-50.9)	1.3 (3.4-0.5)	2.5 (2.3-2.7)	2.5 (2.3-2.7)	19.5 (6.7-52.2)	-0.52	14.4-44.2
CC-BIL	7.50 (7.30-7.70)	10.6 (4.8-20.9)	5.0 (3.6-6.3)	21.8 (21.7-21.7)	2.1 (4.6-1.0)	6.0 (5.5-6.4)	6.0 (5.5-6.4)	29.0 (12.1-61.5)	-0.37	20.8-61.0
SU96-7	8.26 (7.70-8.93)	56.1 (14.9-252.6)	5.0 (5.0-5.0)	54.8 (46.9-66.5)	1.0 (3.1-0.3)	1.0 (0.9-1.1)	1.0 (0.9-0.1)	10.1 (2.9-40.2)	-1	8.1-26.4
BFM-Boss	7.94 (7.31-8.40)	30.6 (4.8-121.1)	4.7 (3.5-7.3)	114.3 (64.7-200.1)	3.7 (13.4-1.7)	7.0 (6.5-7.5)	7.0 (6.5-7.5)	18.7 (4.8-45.5)	-0.55	17.0-51.0
Obi12	8.19 (8.04-8.34)	30.0 (19.9-45.1)	3.2 (3.0-3.3)	55.1 (50.5-59.7)	1.8 (2.5-1.3)	1.9 (1.7-2.0)	1.9 (1.73-2.01)	10.2 (6.8-15.2)	-1	10.3-32.9
Shimizu-do B1	7.76 (7.57-8.18)	14.5 (6.6-49.7)	3.8 (2.9-5.0)	97.9 (93.7-104.2)	6.7 (14.1-2.1)	5.7 (5.4-6.0)	5.7 (5.4-6.0)	8.5 (3.9-28.7)	-1.46	6.2-21.0
Ryuo-do-R1	8.08 (7.82-8.29)	18.0 (9.3-36.6)	2.4 (2.2-3.0)	154.1 (145-168)	8.6 (15.6-4.6)	5.5 (5.2-5.7)	5.5 (5.2-5.7)	6.4 (3.3-12.5)	-1.14	9.2-29.5

Tabulated data are mean values, with the range associated with each parameter presented in parentheses. <sup>a-d</sup> Range represents the spread of values in each measured data set. <sup>e</sup> The range of values associated with the sulphate content of speleothem calcite are calculated based on an instrumental precision of 7.5% RSD from replicate analyses. <sup>f</sup> The range in D<sub>SO4</sub> x 10<sup>5</sup> is calculated based on pairing min and max values of SO<sub>4</sub> and CO<sub>3</sub> in each of the measured data sets. <sup>g</sup> Growth rates are obtained from sources listed in Table 4. <sup>h</sup> The range in expected D<sub>SO4</sub> is calculated from the experimental data on sulphate partitioning extrapolated to appropriate growth rates (Figure 8) at low (2 ppm) and high (20 ppm) aqueous sulphate concentrations.



Table 4

Speleothem code	Cave details	Data source
ASFA 3	Rukiesa cave, Ethiopia. Asfa chamber	a Asrat et al., 2008; b-c Baker et al., 2007; d-e Data source this publication; f Asrat et al., 2008; g calculated from LOG growth rate based on Fig 8
MERC-1	Rukiesa cave, Ethiopia. Merc chamber	a-c Asrat et al., 2008; d-e Data source this publication; f Asrat et al., 2008; g calculated from LOG growth rate based on Fig 8
CC-BIL	Crag cave, Ireland	a-c Baldini et al., 2006; d Data source this publication; e Wynn et al., 2008; f Baldini et al., 2008; g calculated from LOG growth rate based on Fig 8
Assynt	Uamh Am Tartair, Assynt, UK	a-d Fuller et al., 2006; e Data source this publication; f Proctor et al., 2000; g calculated from LOG growth rate based on Fig 8
BFM-Boss	Browns Folly Mine, UK	a-d Data source this publication; e Wynn et al., 2008; f Data source this publication g calculated from LOG growth rate based on Fig 8
Obi12	Obir cave, Austria. Saulenhalle chamber	a-d Fairchild et al., 2010; e Data source this publication; f Fairchild et al., 2010; g calculated from LOG growth rate based on Fig 8
Shimizu-do B	Shimizu-do cave, Japan. Stalagmite B	a-f Uchida et al., 2013; g calculated from LOG growth rate based on Fig 8
Ryuo-do-R1	Ryuo-do cave, Japan	a-f Uchida et al., 2013; g calculated from LOG growth rate based on Fig 8

a = drip water pH, b = drip water carbonate, c = drip water bicarbonate, d = drip water sulphate concentration, e = sulphate concentration in speleothem calcite from the most recent growth, f = speleothem growth rate, g = expected range in  $D_{SO_4}$  calculated from experimental data on sulphate partitioning extrapolated to appropriate growth rates at low (2 ppm) and high (20 ppm) aqueous sulphate concentrations.

Figure S1

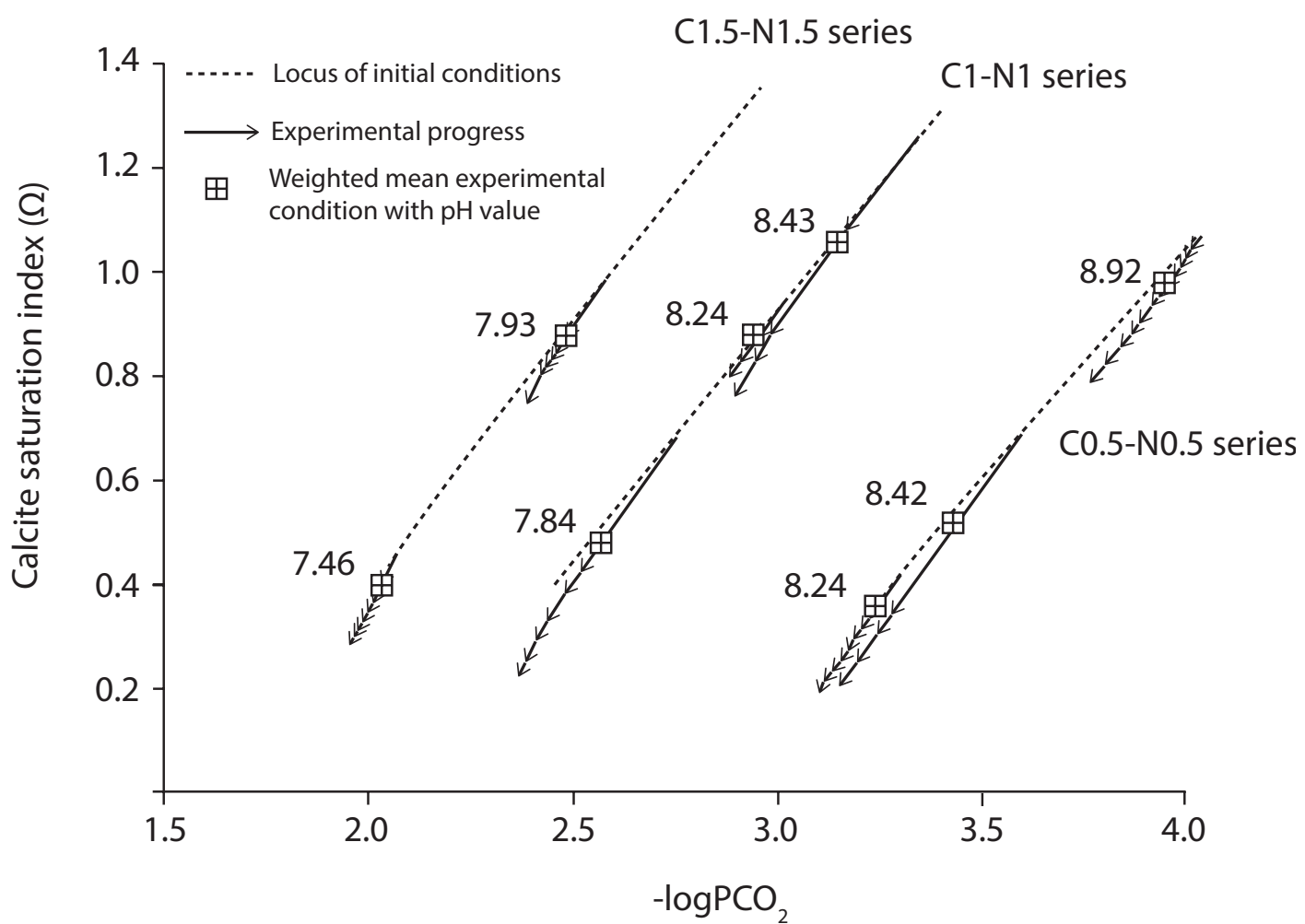


Figure S2

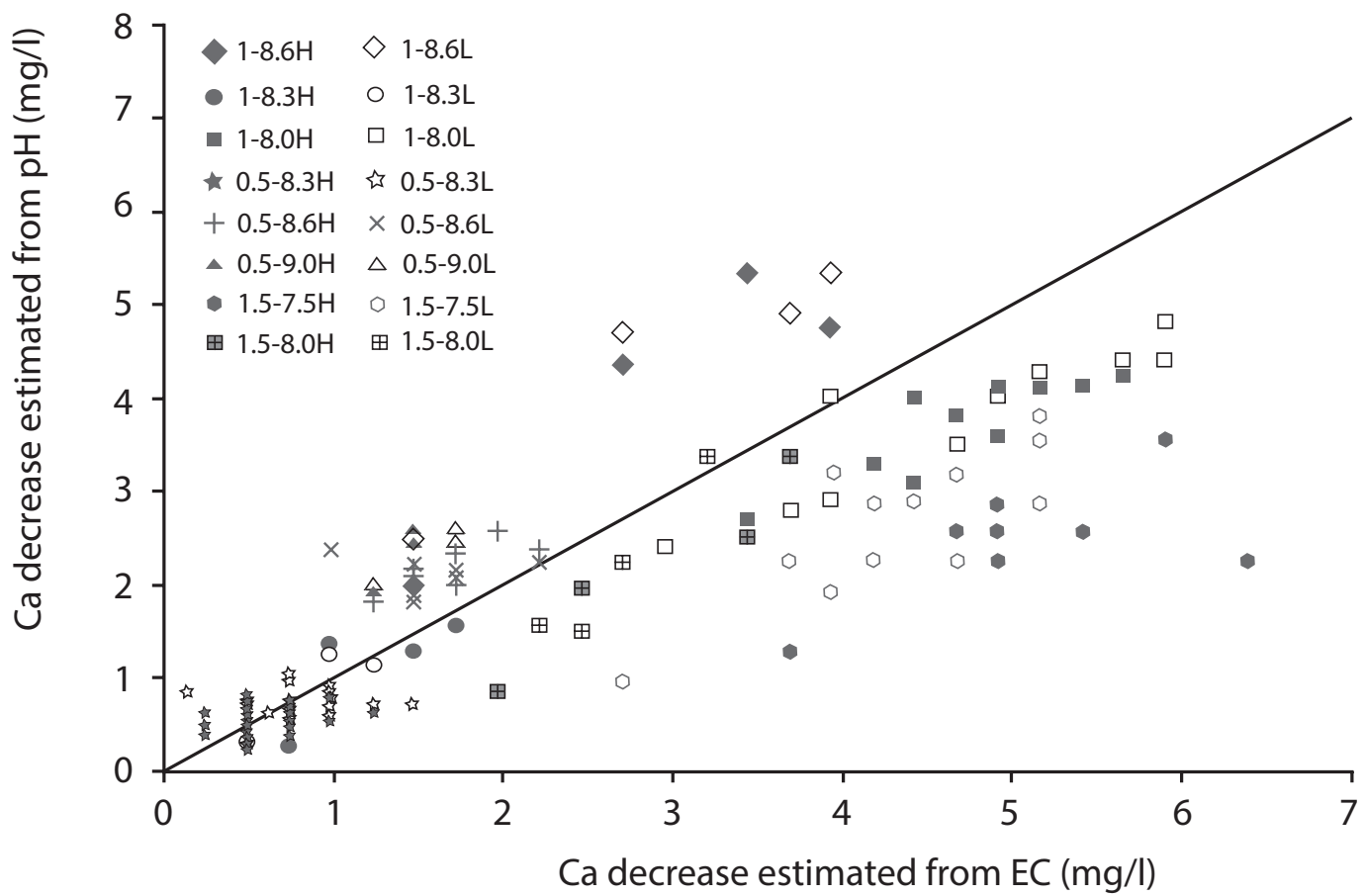
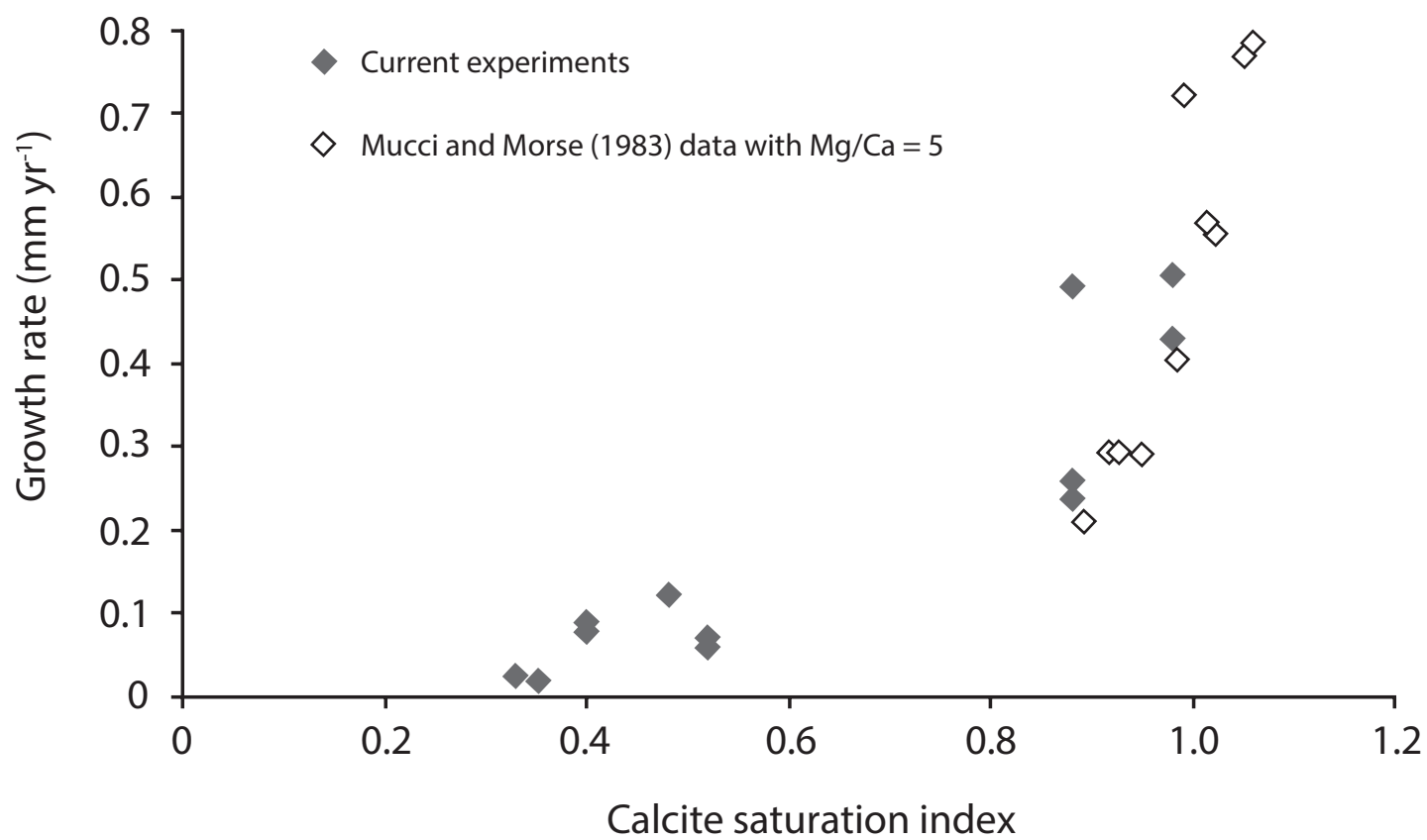


Figure S3



Supplementary text

### **Site and sample description of cave sites containing coeval measurement of drip water and speleothem sulphur concentrations**

Coeval speleothem extraction and drip water chemical monitoring have allowed the calculation of site-specific  $D_{SO_4}$  values at the following cave sites: Rukiesa cave, Ethiopia; Crag Cave, Ireland; Uamh An Tartair, Scotland, UK; Browns Folly Mine, UK; Shimizu-do cave, Japan; and Ryuo-do cave, Japan. The site and sample descriptions at each of these caves is documented as follows:

Rukiesa cave is located within the Jurassic limestone beds of the Mechara karst of the southeastern Ethiopian plateau (Asrat et al., 2007, 2008). The cave system is formed in a linear depression and consists of horizontal chambers radiating from a vertical passageway. The two main chambers were actively monitored between 2003 to 2007 and named as 'Mercury' chamber located at a depth of approximately 25 meters below the entrance, and Asfa chamber at a depth of approximately 30 meters (Asrat et al., 2008). Speleothems were collected from each chamber and named Merc-1 and Asfa-3 respectively. Each speleothem has provided a 100 year record of climate based on growth rate and  $\delta^{18}O_{\text{carbonate}}$  (Baker et al., 2007), and a lipid biomarker record of land use change (Blyth et al. 2007). Sulphur concentration in the most recent growth of each stalagmite was determined using HR-ICPMS following methods detailed in Frisia et al. (2005). Crag cave is developed within the Lower Carboniferous Limestone of County Kerry, Ireland (McDermott et al. 1999; Tooth and Fairchild, 2003; Baldini et al., 2006; Baldini et al. 2008; Sherwin and Baldini, 2011). The sampled stalagmite (CC-Bil) was collected in 2002 and has demonstrated an approximately linear rate of growth for the past 260 years (Baldini et al., 2008). Drip water chemical monitoring was initiated for the drip feeding stalagmite CC-Bil in April 2000, and continued until August 2005, with samples obtained approximately every three months (Baldini et al., 2006; Baldini et al., 2008). Drip rates and calcite deposition were recorded underneath the drip from August 2009 until February 2010, but no detailed water chemistry data was recorded over this interval (Sherwin and Baldini, 2011). The sulphur record contained within CC-Bil is reported within Wynn et al., 2008 and noted to reflect extensive redox cycling in the sediments above the cave. Browns Folly Mine, SW England, is a limestone mine developed in the Jurassic Great Oolite Series and known to be in use between 1836 to 1886 (See Baker et al., 1998, 1999; Baldini et al., 2001; Baldini et al, 2005; Fairchild et al., 2006 for further site details). The speleothem BFM-BOSS was removed in 1996 from a chamber approximately 300 metres into the mine and has provided a record of  $\delta^{13}C$  and  $\delta^{18}O$  between 1916 to 1996 reflecting the development of vegetation across the site since the cessation of mining activity (Baldini et al., 2005). The sulphur record contained within this speleothem is heavily dominated by an anthropogenic pollution signal, reflective of the industrial heritage of the area (Wynn et al., 2008). Uamh An Tartair ('Cave of the Roaring') is located in the NW of Scotland, UK, within the Cambro-Ordovician dolomite of Inchnadamph, Assynt (Proctor et al., 2000; Fuller et al., 2008, Baker et al., 2012). Speleothem SU-96-7 was removed from the cave in 1996 and has since provided a 1000-year record of climate dynamics based on growth rate (Proctor et al., 2000; Baker et al., 2015) and  $\delta^{18}O$  proxies (Baker et al., 2011; 2012). Monitoring of drip water chemistry at site SU-96-7 was undertaken between 2004-2007 and is presented within Fuller (2006). Sulphur concentration in the most recent growth of SU-96-7 was determined using HR-ICPMS following methods detailed in Frisia et al. (2005). The Shimizu-do and Ryuo-do caves are formed within the Palaeogene Nanatsugama calcareous sandstone of Nagasaki, Japan (Uchida et al., 2013).

Speleothems Shimizu-do B and Ryuo-do-R1 were actively growing upon collection and were used to reconstruct vegetation dynamics and sulphur source characteristics over the past 500 years (Uchida et al., 2013). Raw data comprising speleothem and drip water sulphate values (2009-2011) reported in Uchida et al., (2013) allow calculation of  $D_{SO_4}$  values according to the methods presented in this paper for inclusion in the global dataset.